



Trans-Pacific transport and evolution of aerosols: evaluation of quasi-global WRF-Chem simulation with multiple observations

Zhiyuan Hu^{1,2}, Chun Zhao², Jianping Huang¹, L. Ruby Leung², Yun Qian², Hongbin Yu^{3,4}, Lei Huang⁵, and Olga V. Kalashnikova⁵

¹Key Laboratory for Semi-Arid Climate Change of the Ministry of Education, Lanzhou University, Gansu, China

²Atmospheric Sciences and Global Change Division, Pacific Northwest National Laboratory, Richland, WA, USA

³Earth System Science Interdisciplinary Center, University of Maryland, College Park, MD, USA

⁴Earth Science Division, NASA Goddard Space Flight Center, Greenbelt, MD, USA

⁵Jet Propulsion Laboratory, California Institute of Technology and NASA, Pasadena, CA, USA

Correspondence to: Chun Zhao (chun.zhao@pnnl.gov)

Received: 19 November 2015 – Published in Geosci. Model Dev. Discuss.: 19 January 2016

Revised: 12 April 2016 – Accepted: 14 April 2016 – Published: 10 May 2016

Abstract. A fully coupled meteorology-chemistry model (WRF-Chem, the Weather Research and Forecasting model coupled with chemistry) has been configured to conduct quasi-global simulation for 5 years (2010–2014) and evaluated with multiple observation data sets for the first time. The evaluation focuses on the simulation over the trans-Pacific transport region using various reanalysis and observational data sets for meteorological fields and aerosol properties. The simulation generally captures the overall spatial and seasonal variability of satellite retrieved aerosol optical depth (AOD) and absorbing AOD (AAOD) over the Pacific that is determined by the outflow of pollutants and dust and the emissions of marine aerosols. The assessment of simulated extinction Ångström exponent (EAE) indicates that the model generally reproduces the variability of aerosol size distributions as seen by satellites. In addition, the vertical profile of aerosol extinction and its seasonality over the Pacific are also well simulated. The difference between the simulation and satellite retrievals can be mainly attributed to model biases in estimating marine aerosol emissions as well as the satellite sampling and retrieval uncertainties. Compared with the surface measurements over the western USA, the model reasonably simulates the observed magnitude and seasonality of dust, sulfate, and nitrate surface concentrations, but significantly underestimates the peak surface concentrations of carbonaceous aerosol likely due to model biases in the spatial and temporal variability of biomass burning emissions and secondary organic aerosol (SOA) production. A sen-

sitivity simulation shows that the trans-Pacific transported dust, sulfate, and nitrate can make significant contribution to surface concentrations over the rural areas of the western USA, while the peaks of carbonaceous aerosol surface concentrations are dominated by the North American emissions. Both the retrievals and simulation show small interannual variability of aerosol characteristics for 2010–2014 averaged over three Pacific sub-regions. The evaluation in this study demonstrates that the WRF-Chem quasi-global simulation can be used for investigating trans-Pacific transport of aerosols and providing reasonable inflow chemical boundaries for the western USA, allowing one to further understand the impact of transported pollutants on the regional air quality and climate with high-resolution nested regional modeling.

1 Introduction

Aerosols, originating from natural and anthropogenic sources in Europe, North Africa, and East Asia, can be transported thousands of miles downwind across the Pacific Ocean to North America and even beyond. Previous studies using ground-based and satellite measurements and numerical models have estimated about 7–10 days of travel time for aerosols to traverse the Pacific Ocean (Eguchi et al., 2009). Previous studies have shown that aerosols outflowed from the Asian continent could be transported by the mid-latitude

prevailing westerlies across the Pacific Ocean and ultimately reach the west coast of North America and beyond, and its efficiency is the largest in spring (e.g., Takemura et al., 2002; Chin et al., 2007; Huang et al., 2008; Yu et al., 2008; Uno et al., 2009, 2011; Alizadeh-Choobari et al., 2014). Takemura et al. (2002) found that the contribution of anthropogenic aerosols to the total aerosol optical thickness is comparable to that of dust during the transport over the North Pacific in spring. Chin et al. (2007) found that the long-range transported dust brought 3 to 4 times more fine particles than anthropogenic pollutants to the total surface fine particles over the USA on annual average with a maximum influence in spring, and over the northwestern USA Yu et al. (2008) estimated that about 25 % of the Asian outflow reaches the west coast of North America, which is about 15 % of the total North American emissions; the transport fluxes are largest in spring and smallest in summer. Uno et al. (2011) also revealed that the dust trans-Pacific path sometimes could be split into two branches: a southern path to the central USA and a northern path that is trapped and stagnant for a longer time and finally subsides over the northwestern USA.

These trans-Pacific aerosols can play an important role in atmospheric composition (e.g., Yu et al., 2008), air quality (e.g., Jaffe et al., 1999; VanCuren, 2003; Heald et al., 2006; Chin et al., 2007; Fischer et al., 2009; Yu et al., 2012; Tao et al., 2016), and regional weather and climate (e.g., Lau et al., 2008; Eguchi et al., 2009; Yu et al., 2012; Creamean et al., 2013; Fan et al., 2014; Huang et al., 2006, 2014) over the US West Coast. At the surface, Heald et al. (2006) found that Asian anthropogenic aerosol plume increased aerosol concentrations in elevated regions of the northwestern USA by $0.16 \mu\text{g m}^{-3}$ in spring 2001. Chin et al. (2007) also found that long-range transported dust increased the annual mean fine particle concentrations by $0.5\text{--}0.8 \mu\text{g m}^{-3}$ over the western USA, with a maximum enhancement in spring. The trans-Pacific transported aerosols can also significantly absorb and scatter solar radiation (Yu et al., 2012; Fast et al., 2014; Tao et al., 2016), and serve as cloud condensation nuclei and ice nuclei that affect winter storms in the western USA (Sassen, 2002; Ault et al., 2011; Creamean et al., 2013; Fan et al., 2014). Deposition of the transported aerosols on/into snowpack in elevated regions (Hadley et al., 2010) may also accelerate snowmelt and influence the regional hydrological cycle and climate over the western USA (Qian et al., 2009, 2015; Painter et al., 2010). Hence it is important to quantify the trans-Pacific transport of aerosols and how they evolve over the long distance.

Previous studies have used global models to quantify the long-range transport of aerosols to the western USA (e.g., Fairlie et al., 2007; Heald et al., 2006; Chin et al., 2007; Hadley et al., 2007). However, simulations were performed at relatively coarse resolutions (typically 1–2 degrees) that cannot fully resolve the large geographical variability of aerosols over the western USA with complex topography (Zhao et al., 2013a). Coarse-resolution simulations also lack the capabil-

ity to fully resolve aerosol–cloud–precipitation interaction. Some studies have reported regional simulations at relatively high resolutions over the western USA (e.g., Zhao et al., 2013a; Fan et al., 2014; Fast et al., 2014). However, most of them either used sparse in situ observations to provide lateral boundary conditions that are only suitable for idealized or short-term sensitivity studies, or used simulations from global models with inconsistent physics and chemistry schemes to provide lateral boundary conditions, which introduce biases in estimating the contribution and effect of trans-Pacific transported aerosols.

To investigate the impact of trans-Pacific transported aerosols on regional air quality and climate of the US West Coast, a multi-scale modeling framework including global simulation at coarse resolutions that captures the large-scale circulation and provides consistent chemical lateral boundaries for nested regional simulation at high resolutions is needed. WRF-Chem, the Weather Research and Forecasting (WRF) model (Skamarock et al., 2008) coupled with a chemistry component (Grell et al., 2005), is such a modeling framework. As a state-of-the-art model, WRF-Chem supports nested simulations, and includes complex aerosol processes and interactions between aerosols and radiation, clouds, and snow albedo (Zhao et al., 2014). The model has been used extensively to study aerosols and their impacts on air quality and climate at regional scales (e.g., Fast et al., 2006, 2009; Gustafson et al., 2007; Qian et al., 2010; Gao et al., 2011, 2014; Shrivastava et al., 2011; Chen et al., 2013, 2014; Zhao et al., 2010a, 2011, 2012, 2013a, 2014). Zhao et al. (2013b) is the first study to use WRF-Chem for quasi-global ($180^\circ\text{W}\text{--}180^\circ\text{E}$, $60^\circ\text{S}\text{--}70^\circ\text{N}$) simulations at a resolution of $1^\circ \times 1^\circ$ to examine uncertainties in simulating global dust mass balance and radiative forcing.

Although the quasi-global WRF-Chem simulation described by Zhao et al. (2013b) has been used to provide realistic chemical lateral boundary conditions for multiple regional modeling studies (e.g., Zhao et al., 2014; Fan et al., 2015), its evaluation has not been documented so far. In this study, the WRF-Chem simulation for 2010–2014 is evaluated extensively using observational data. For lack of in situ observations over East Asia and the Pacific Ocean during our simulation period, evaluation is performed mainly using reanalysis and satellite retrieval (e.g., CALIPSO, MODIS, and MISR; see Sect. 3.1 for further definition.) data sets, along with some available ground-based observations from AEROSOL ROBOTIC NETWORK (AERONET) and Interagency Monitoring for Protected Visual Environments (IMPROVE) in the region. We focus on the simulation over the trans-Pacific transport region as a first step to evaluate the simulation for providing consistent lateral chemical boundaries for nested regional simulations used to investigate the impact of transported aerosols on regional air quality and climate. Spatial evolution of aerosols during the trans-Pacific transport as well as their seasonal and annual variability simulated by WRF-Chem will also be characterized.

In the following sections, the detailed setup of WRF-Chem will be described in Sect. 2. In Sect. 3 ground-based measurements and satellite retrievals will be presented. In Sect. 4, we evaluate the WRF-Chem simulated spatial distributions and seasonal and annual variability of aerosols across the Pacific with the observations. The conclusion can be found in Sect. 5.

2 Model description

2.1 WRF-Chem

In this study, WRF-Chem (3.5.1), updated by scientists at Pacific Northwest National Laboratory (PNNL), is used. The MOSAIC (Model for Simulation Aerosol Interactions and Chemistry) aerosol module (Zaveri et al., 2008) coupled with the CBM-Z (carbon bond mechanism) photochemical mechanism (Zaveri and Peters, 1999) in WRF-Chem is selected in this study. MOSAIC uses a sectional approach to represent aerosol size distributions with four or eight discrete size bins in the current version of WRF-Chem (Fast et al., 2006). All major aerosol components including sulfate (SO_4^{-2}), nitrate (NO_3^-), ammonium (NH_4^+), black carbon (BC), organic matter (OM), sea-salt, mineral dust, and other inorganic matter (OIN) are simulated in the model. The MOSAIC aerosol scheme includes physical and chemical processes of nucleation, condensation, coagulation, aqueous phase chemistry, and water uptake by aerosols. Dry deposition of aerosol mass and number is simulated following the approach of Binkowski and Shankar (1995), which includes both turbulent diffusion and gravitational settling. Wet removal of aerosols by grid-resolved stratiform clouds and precipitation includes in-cloud removal (rainout) and below-cloud removal (washout) by impaction and interception, following Easter et al. (2004) and Chapman et al. (2009). Cloud-ice-borne aerosols through ice nucleation of aerosols are not considered in the model, but the removal of aerosols by the droplet freezing process is considered. Convective transport and wet removal of aerosols by cumulus clouds follow Zhao et al. (2013b).

Aerosol optical properties such as extinction, single scattering albedo (SSA), and asymmetry factor for scattering are computed as a function of wavelength for each model grid box. Aerosols are assumed internally mixed in each bin (i.e., a complex refractive index is calculated by volume averaging for each bin for each chemical constituent of aerosols). The Optical Properties of Aerosols and Clouds (OPAC) data set (Hess et al., 1998) is used for the shortwave (SW) and longwave (LW) refractive indices of aerosols, except that a constant value of $1.53 + 0.003i$ is used for the SW refractive index of dust following Zhao et al. (2010a, 2011). A detailed description of the computation of aerosol optical properties in WRF-Chem can be found in Fast et al. (2006) and Barnard et al. (2010). Aerosol radiative feedback is coupled with the

Rapid Radiative Transfer Model (RRTMG) (Mlawer et al., 1997; Iacono et al., 2000) for both SW and LW radiation as implemented by Zhao et al. (2011). The optical properties and direct radiative forcing of individual aerosol species in the atmosphere are diagnosed following the methodology described in Zhao et al. (2013a). Aerosol–cloud interactions were included in the model by Gustafson et al. (2007) for calculating the activation and resuspension between dry aerosols and cloud droplets.

2.2 Numerical experiments

Following Zhao et al. (2013b), we use a quasi-global channel configuration with periodic boundary conditions in the zonal direction and 360×145 grid cells (180°W – 180°E , 67.5°S – 77.5°N) to perform simulation at 1° horizontal resolution over the period 2010–2014. Alizadeh-Choobari et al. (2015) conducted a global WRF-Chem simulation of dust and its radiative forcing, which was configured with dust aerosol only without other aerosols and chemistry. However, WRF-Chem global simulation with sophisticated chemistry including anthropogenic and natural aerosols could not run stably due potentially to convergence issue of solving chemical reactions near the relatively pristine polar regions. Given the need of sophisticated chemistry to simulate not only dust but also other anthropogenic aerosols, a more stable near-global coverage WRF-Chem configuration is used in this study to circumvent this technical difficulty to characterize the trans-Pacific transport of aerosols. The simulation is configured with 35 vertical layers up to 50 hPa. The meteorological initial and lateral meridional boundary conditions are derived from the National Center for Environmental Prediction final analysis (NCEP/FNL) data at 1° horizontal resolution and 6 h temporal intervals. The modeled wind components u and v and atmospheric temperature are nudged towards the NCEP/FNL reanalysis data throughout the domain with a nudging timescale of 6 h in all cases (Stauffer and Seaman, 1990). This provides a more realistic simulation of large-scale circulation, which is important for modeling long-range transport. The chemical initial and meridional boundary conditions are taken from the default profiles in WRF-Chem, which are the same as those used by McKeen et al. (2002) and are based on averages of mid-latitude aircraft profiles from several field studies over the eastern Pacific Ocean. The impact of chemical boundary conditions on the simulated results is negligible (Zhao et al., 2013b). This study uses a set of selected schemes for model physics, including the MYJ (Mellor–Yamada–Janjic) planetary boundary layer scheme, Noah land surface scheme, Morrison 2-moment microphysics scheme, Kain–Fritsch cumulus scheme, and RRTMG longwave and shortwave radiation schemes.

2.3 Emissions

Anthropogenic emissions are obtained from the REanalysis of the TROpospheric (RETRO) chemical composition inventories (Schultz et al., 2007; http://retro-archive.iek.fz-juelich.de/data/documents/reports/D1-6_final.pdf) except over East Asia and the United States. Over the USA, the National Emission Inventory (NEI) 2011 is used. Over East Asia, the Asian emission inventory described by Zhang et al. (2009) at $0.5^\circ \times 0.5^\circ$ horizontal resolution for 2006 is used, but BC, OM, and sulfate emissions over China are from the China emission inventory for 2010 described by Lu et al. (2011) at a $0.1^\circ \times 0.1^\circ$ horizontal spatial resolution and a monthly temporal resolution for the simulation period. Biogenic emissions are calculated following Guenther et al. (1994). Biomass burning emissions are obtained from the Global Fire Emissions Database, version 3 (GFEDv3) with monthly temporal resolution (van der Werf et al., 2010) and vertically distributed following the injection heights suggested by Dentener et al. (2006) for the Aerosol Comparison between Observations and Models (AeroCom) project. The WRF-Chem code is modified to update the biomass burning emissions every day. Sea-salt emission follows Zhao et al. (2013a), which is based on Gong (2003) to include the correction of particles with a radius less than $0.2 \mu\text{m}$ and Jaeglé et al. (2011) to include the sea-salt emission dependence on sea surface temperature. Vertical dust emission fluxes are calculated with the Goddard Chemical Aerosol Radiation Transport (GOCART) dust emission scheme (Ginoux et al., 2001), and the emitted dust particles are distributed into the MOSAIC aerosol size bins following a theoretical expression based on the physics of scale-invariant fragmentation of brittle materials derived by Kok (2011). For MOSAIC 8 bin, dust particles are emitted into eight size bins with mass fractions of 10^{-6} , 10^{-4} , 0.02, 0.2, 1.5, 6, 26, and 45 %. Although the main purpose of this study is to evaluate the WRF-Chem simulation, a sensitivity simulation, in which dust, fire, and anthropogenic emissions over North America ($10\text{--}70^\circ \text{N}$ and $170\text{--}60^\circ \text{W}$) are removed, is also conducted to understand the contribution of trans-Pacific transported aerosols to the surface aerosol concentrations over the western USA.

3 Aerosol observations

3.1 Satellite retrievals

3.1.1 MODIS

The Moderate Resolution Imaging SpectroRadiometer (MODIS) instrument onboard the NASA EOS Terra satellite observes Earth in 36 spectral bands from 0.4 to $14.4 \mu\text{m}$, and provides nearly daily global coverage with a local equatorial overpass time of about 10:30 LT (local time) since 2000 (King et al., 1999). The “dark target” algorithm has been developed to retrieve aerosol optical depth (AOD) and size

parameters (Ångström exponent, effective radius, and fine-mode fraction) over waters and vegetated lands (Kaufman et al., 1997; Remer et al., 2005). The “deep blue” algorithm has been implemented to retrieve AOD over bright land initially, which then has also been extended to vegetated land (Hsu et al., 2006, 2013). MODIS aerosol products have been widely used to characterize the regional, seasonal, and global distribution of aerosol and its components (Yu et al., 2003, 2009; Chin et al., 2004; Kaufman et al., 2005a), estimate aerosol radiative forcing (Yu et al., 2004; Remer and Kaufman, 2006), and study aerosol–cloud interactions (Kaufman et al., 2005b; Koren et al., 2005; Yu et al., 2007). In this study, MODIS data from the collection 5.1 are used. We use the “deep blue” AOD over land and the “dark target” AOD over ocean, both at 550 nm and at $1^\circ \times 1^\circ$ horizontal resolution. Also, we use the “dark target” over-ocean extinction Ångström exponent (EAE) over the $470\text{--}660 \text{ nm}$ wavelength range to evaluate model simulations of particle size information (Anderson et al., 2005; Remer et al., 2005; Levy et al., 2013).

3.1.2 MISR

The Multi-angle Imaging SpectroRadiometer (MISR) instrument onboard the Terra spacecraft crosses the Equator at $\sim 10:30 \text{ LT}$ since 1999. It observes continuously in four narrow spectral bands centered at 446 , 558 , 672 , and 866 nm using nine separate cameras oriented along the orbital track with surface viewing zenith angles ranging from $\pm 70.5^\circ$ (Diner et al., 1998). Aerosol retrievals are performed on 16×16 patches of 1.1 km sub-regions, yielding an aerosol product at $17.6 \text{ km} \times 17.6 \text{ km}$ spatial resolution, referred to as a “level 2” product (Martonchik et al., 2002). MISR level 2 aerosol products have been described in Kahn et al. (2009). The latest version (version 22) of MISR aerosol product also provides the fraction of AOD due to “fine” (particle radii $< 0.35 \mu\text{m}$), “medium” (particle radii between 0.35 and $0.7 \mu\text{m}$), and “large” (particle radii $> 0.7 \mu\text{m}$) particles as well as the fraction of AOD due to “spherical” and “nonspherical” particles at the four MISR spectral bands. Here, we compare the MISR AOD at 550 nm from version 22 of level 2 with the model results.

3.1.3 OMI

The Ozone Monitoring Instrument (OMI) onboard the NASA Aura satellite has a daily global coverage, and crosses the Equator at $13:45 \text{ LT}$. The nadir horizontal resolution of OMI is $24 \text{ km} \times 13 \text{ km}$. In this study the OMI/Aura Near-UV Aerosol Absorption and Extinction Optical Depth and Single Scattering Albedo product (OMAERUV) level 2 collection 003 v1.4.2 product (Jethva et al., 2014) is used as an independent data set providing SSA that is derived based on the reflectances measured by the OMI instrument at $0.39 \mu\text{m}$. The information on aerosol absorption in OMI measurements comes, to a large extent, from the interac-

tion with Rayleigh scattering in the UV spectral region (Torres et al., 2013). The retrieved parameters are also reported at 0.38 and 0.50 μm . Current OMI AOD has positive biases likely due to a combination of factors including cloud contamination, surface albedo effects, radiometric calibrations, and misidentified aerosol type (Ahn et al., 2008). Therefore, in this study, OMI absorbing AOD (AAOD) at 500 nm is reconstructed using the WRF-Chem simulated 500 nm AOD and OMI SSA at 500 nm with the formula of $\text{AAOD}_{\text{OMI}} = \text{AOD}_{\text{MODEL}} \times (1 - \text{SSA}_{\text{OMI}})$.

3.1.4 CALIPSO

In this study, we use aerosol extinction profiles retrieved by the Cloud–Aerosol Lidar with Orthogonal Polarization (CALIOP) onboard the Cloud–Aerosol Lidar and Infrared Pathfinder Satellite Observation (CALIPSO) satellite. The CALIPSO satellite was launched into a Sun-synchronous orbit on 28 April 2006. CALIOP is a dual-wavelength polarization lidar and is designed to acquire vertical profiles of attenuated backscatter from a near-nadir-viewing geometry during both day and night phase (Winker et al., 2007; Liu et al., 2004, 2008; Hu et al., 2007, 2009). In this study, the aerosol extinction profiles at a nominal horizontal resolution of 5 km from the CALIPSO level 2 profile products are used to evaluate the model. We focus on the CALIOP nighttime observations in cloud-free condition, because nighttime observations have higher accuracy than daytime observations (Winker et al., 2009).

The cloud–aerosol discrimination (CAD) score, which is an indicator that measures confidence level of the discrimination between clouds (positive value) and aerosols (negative value), is used to help screen out aerosol profiles that contain cloud signals. We include the aerosol data with CAD score between -20 and -100 , the same as Yu et al. (2010, 2015). The other screening is to exclude aerosol layers where the retrieval algorithm has to adjust the initially selected lidar ratio that is based on the type and subtype of the aerosol layer to be analyzed. It should be noted that when the aerosol extinction is not detected by CALIOP, we set its value and also the corresponding model result equal to zero, and then we compare CALIOP extinction profiles with the model and analyze the seasonal variation.

3.2 Ground-based observations

3.2.1 AERONET

The AERONET is a globally distributed remote sensing network for aerosol monitoring from ground stations (Holben et al., 1998). AERONET uses the Cimel sun–sky photometer that measures AOD in 16 spectral channels (340–1640 nm). The measurements provide products every 15 min during daytime. In addition, an inversion algorithm is used for the retrieval of aerosol size distribution, complex refractive in-

dex, single-scattering albedo, and phase function (Dubovik and King, 2000; Dubovik et al., 2002). The spectral AOD from AERONET has an accuracy of ± 0.01 (Eck et al., 1999; Holben et al., 2001). In the analysis presented in this paper, the cloud screened and quality assured level 2.0 products are used. AERONET products do not measure at wavelength 0.55 μm , so we calculate them through using the Ångström exponent and the values at two nearest wavelengths 0.5 and 0.675 μm . The AERONET sites are located along the trans-Pacific transport pathways, so the products are important for evaluating the model results. Five sites over East Asia, one island site over the North Pacific, and four sites over the western USA are selected for comparison as shown in Fig. 1.

3.2.2 IMPROVE

The IMPROVE network was initiated in 1985 by US federal agencies including EPA, National Park Services, Department of Agriculture–Forest Service, and other land management agencies as a part of the EPA Regional Haze program (Malm et al., 1994). The network monitors the visibility conditions and changes in national parks and wilderness areas on a long-term basis. The detail sample collection and analytical methodology have been given by Hand et al. (2011), and the data can be downloaded from <http://views.cira.colostate.edu/fed/DataWizard/Default.aspx>. There are 15 sites (Fig. 1) along the western coast selected to compare with the surface aerosols of the model. In this study, the mass concentrations of sulfate, nitrate, EC, OM, and dust in $\text{PM}_{2.5}$ (particulate matter with aerodynamic diameter less than 2.5 μm) are used to evaluate the model. Most IMPROVE data were directly downloaded, except for OM and dust. Because IMPROVE reports only organic carbon (OC) measurements, in this study we multiply the OC data by 1.4 for converting measured OC to OM (to account for hydrogen, oxygen, etc.) (Chow et al., 2006; Zhao et al., 2013a). The fine dust is calculated following the formula (Malm et al., 1994; Zhao et al., 2013a)

$$\text{PM}_{2.5} - \text{Dust} = 2.2[\text{Al}] + 2.49[\text{Si}] + 1.63[\text{Ca}] + 2.42[\text{Fe}] + 1.94[\text{Ti}], \quad (1)$$

where [Al], [Si], [Ca], [Fe], and [Ti] represent the mass concentration of aluminum, silicon, calcium, iron, and titanium, respectively.

4 Results

4.1 Wind fields and precipitation

Winds and precipitation are two crucial meteorological factors playing important roles in aerosol emission, transport, and removal. The seasonal mean wind fields at 850 hPa averaged for the period 2010–2014 from the WRF-Chem simulation are compared with the Modern-Era Retrospective

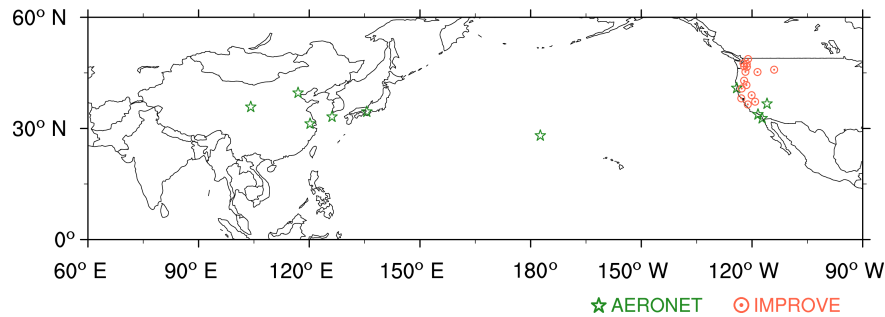


Figure 1. Observation sites for the AERONET (green stars) and IMPROVE (red-dotted circles) networks used in this study.

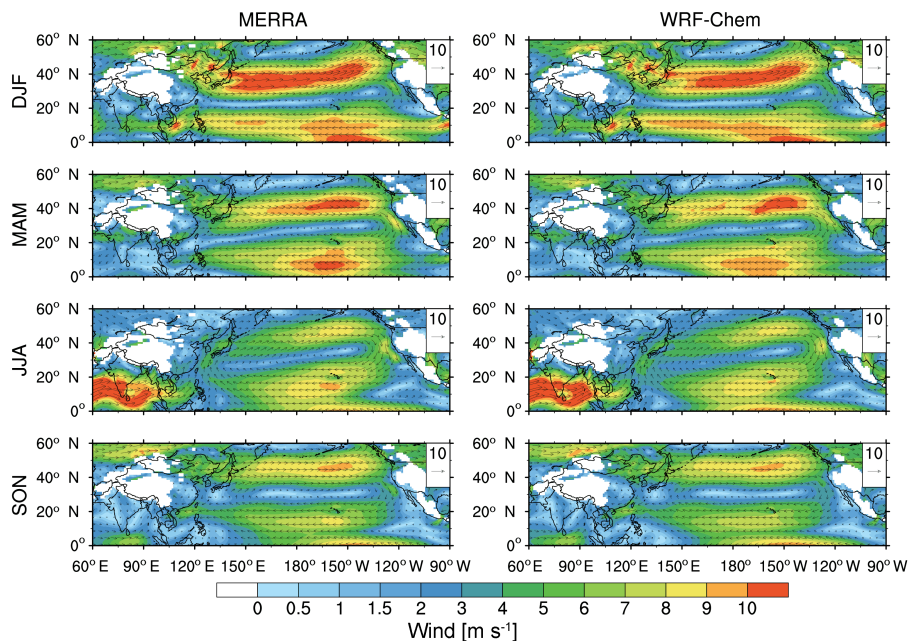


Figure 2. Spatial distributions of seasonal-averaged wind fields at 850 hPa from the MERRA reanalysis and the WRF-Chem simulation for the period 2010–2014.

analysis for Research and Applications (MERRA) reanalysis data (Rienecker et al., 2011) (Fig. 2). Strong westerly winds occur over the North Pacific throughout the seasons with a peak (up to 12 m s^{-1} ; 5.48 m s^{-1} on spatial average) in boreal winter (DJF) followed by boreal spring (MAM) (4.46 m s^{-1} on spatial average). The winds are weakest in boreal fall (SON) (4.1 m s^{-1} on spatial average). In general, the model can well reproduce the spatial pattern of winds across the Pacific with wind speeds of $4.1\text{--}5.41 \text{ m s}^{-1}$ averaged spatially for the four seasons, with a spatial correlation coefficient of 0.98 throughout the seasons. Figure 3 shows the spatial distribution of seasonal mean precipitation from the Global Precipitation Climatology Project (GPCP) observation (Huffman et al., 2001) averaged for the period 2010–2014 and the difference in the WRF-Chem simulation. Over East Asia, precipitation reaches a maximum during the boreal summer (JJA) followed by MAM. In the North Pa-

cific basin, the largest precipitation occurs in DJF along the storm tracks with the maximum westerlies. Over the US West Coast, precipitation peaks during DJF and reaches a minimum in JJA. The simulation reasonably reproduces the spatial and seasonal variations of precipitation with spatial correlation coefficients of 0.89, 0.81, 0.81, and 0.84 for DJF, MAM, JJA, and SON, respectively. The simulation overestimates annual mean precipitation averaged over the North Pacific (3.1 and 4.2 mm day^{-1} , respectively, from GPCP and WRF-Chem). The overestimation (more than 50 %) is particularly over the Inter-Tropical Convergence Zone (ITCZ) and the western tropical Pacific that are south to the 20° N and the major pathway of trans-Pacific transport. The excessive precipitation over the tropical Pacific may be due to biases from the convective parameterizations in producing tropical precipitation in WRF, such as overestimation of precipitation efficiency from the simple treatment of cloud microphysical

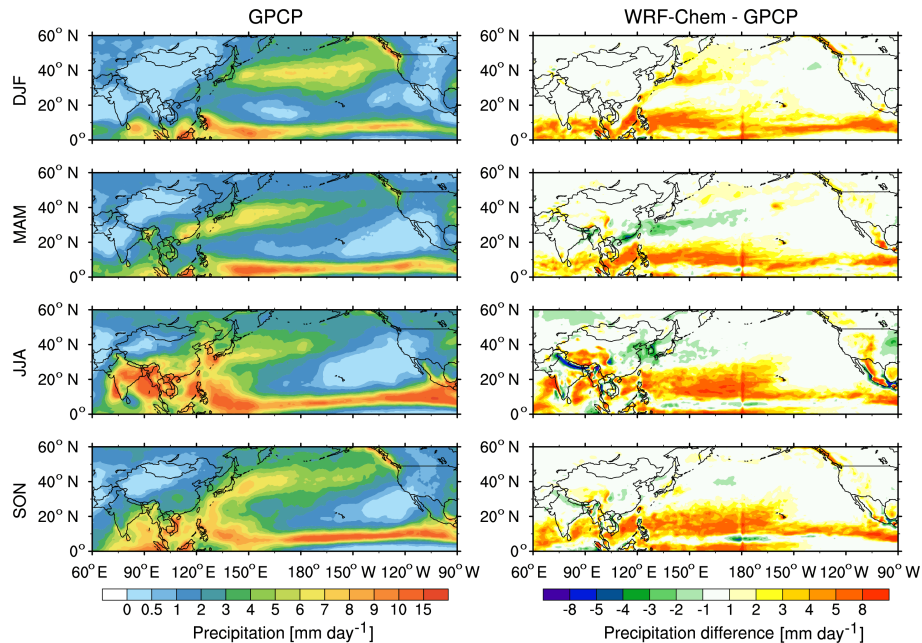


Figure 3. Spatial distributions of seasonal-averaged precipitation from the GPCP observation and the difference between observation and simulation for the period 2010–2014.

processes in convective clouds, and biases in the prescribed temperature and humidity reference profiles (e.g., Fonseca et al., 2015; Hagos et al., 2016). Short sensitivity experiments we performed show that the WRF simulated tropical precipitation is sensitive to the choice of convective parameterizations (not shown).

4.2 Aerosol optical depth

4.2.1 Spatial and temporal variation

Figure 4 shows the spatial distributions of seasonal mean AOD at 550 nm across the Pacific from Asia to North America averaged for 2010–2014 from the retrievals of MODIS and MISR onboard Terra and the corresponding WRF-Chem simulation. The WRF-Chem simulated AOD at 600 and 400 nm are used to derive the AOD at 550 nm (using the Ångström exponent). In order to reduce the sampling discrepancy between the two retrievals, the daily results from the two satellite retrievals and simulation are sampled and averaged at the same time and location. This way of averaging leads to the blank areas of missing values, which are relatively large in JJA. Satellite retrievals show consistent spatial patterns with the spatial correlation coefficients of 0.65–0.88 for the four seasons. The MODIS retrieval shows higher AOD over the semi-arid regions (e.g., Northwest China and the southwestern USA) than the MISR retrieval; however, the MODIS retrieved AOD magnitude over these regions is significantly overestimated because of its large uncertainties in the assumed surface reflectance in semi-arid regions (Remer et al., 2005; Levy et al., 2013). In comparison, the MISR ob-

servations in the western USA show better quality presumably because of the multi-angle capability that allows for a better characterization of surface reflectance. Both retrievals indicate that AOD is high over the Asian continent and gradually decreases across the Pacific. High AOD coincides with the sub-tropical jet (30–50° N, Fig. 2) over the Pacific and results from wind-induced increase in sea-salt loading and the Asian pollutant outflow. Seasonal variation of aerosols across the Pacific is evident, with peak AOD over the western Pacific in MAM and minimum AOD in JJA and SON. This seasonal variation is generally consistent with previous studies (Yu et al., 2008, 2012), although our sampling method results in more missing data from satellite retrievals in JJA than other seasons. Previous studies found that trans-Pacific transport of air pollutants is most efficient in MAM due to active cyclonic activity and that pollutants are lifted to the free troposphere where they can be rapidly transported across the Pacific by strong westerlies (e.g., Forster et al., 2004; Liang et al., 2004; Heald et al., 2006; Yu et al., 2008).

The WRF-Chem simulation generally well captures the observed spatial and seasonal variability of AOD across the Pacific with the spatial correlation coefficients of 0.63–0.76 for the four seasons against the MISR retrievals. The model generally underestimates the retrieved AOD over the North Pacific (0–60° N, 120° E–120° W) with an annual mean value of 0.11, which is lower than the retrieved values of 0.14 (MODIS) and 0.15 (MISR). Over the region north of 20° N (20–60° N, 120° E–120° W), the simulation produces an average AOD of 0.14 that is more consistent with the retrieved values of 0.15 (MODIS) and 0.16 (MISR). This neg-

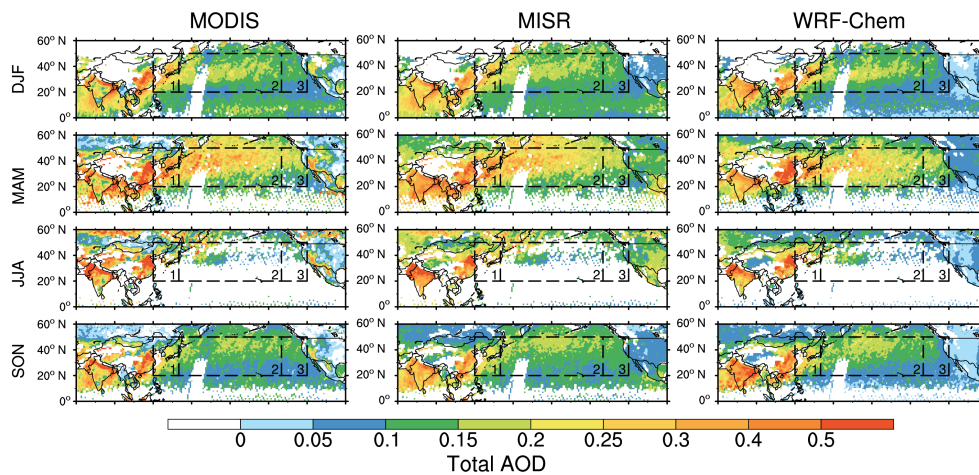


Figure 4. Spatial distributions of seasonal mean 550 nm AOD from the retrievals of MODIS and MISR onboard Terra and the WRF-Chem simulation for the period 2010–2014. The daily results from MISR, MODIS, and WRF-Chem are only sampled for averaging when all of them have valid values at the same location and time. Three sub-regions are denoted by the black boxes: region 1 (20–50° N and 120–140° E), region 2 (20–50° N and 140° E–140° W), and region 3 (20–50° N and 140–120° W).

ative bias of the oceanic AOD south of 20° N may be due to underestimation of marine emissions (Yu et al., 2003) and/or overestimation of aerosol wet removal associated with the positive bias in precipitation (Fig. 3). The discrepancy may also be due to the higher uncertainty at a low aerosol level (Levy et al., 2013) and cloud contamination in the retrievals that leads to an overestimation of AOD in some regions of the North Pacific (e.g., Zhang and Reid, 2006). The model also simulates lower AOD over the continent of North America compared with satellite retrievals. The difference between the simulation and retrievals may be due to the uncertainty in satellite retrievals over the continents (e.g., Liu et al., 2004; Levy et al., 2010).

Since this study focuses on the trans-Pacific transport and evolution of aerosols, the Pacific is further divided into three sub-regions (region 1: 20–50° N and 120–140° E; region 2: 20–50° N and 140° E–140° W; region 3: 20–50° N and 140–120° W) representing the western Pacific, the central Pacific, and the eastern Pacific shown as the black boxes in Fig. 4 for analysis. Figure 5 shows the seasonal mean 550 nm AOD over the three sub-regions from the MISR and MODIS retrievals and the corresponding WRF-Chem simulation at the pass time of MISR and MODIS, respectively, averaged for 2010–2014. The retrievals show clearly that AOD peaks in MAM followed by DJF in all the regions across the Pacific. The simulated annual mean AOD of 0.21, 0.16, and 0.09 over the western, central, and eastern Pacific, respectively, successfully reproduce the observed values of 0.22, 0.16, and 0.10 from MODIS and 0.21, 0.16, and 0.10 from MISR. The simulation also captures the seasonal variability with the maximum AOD in MAM followed by DJF. In general, the MODIS and MISR retrievals and simulation consistently show that AOD reduces from the western Pacific to the eastern Pacific. The interannual variability of AOD over

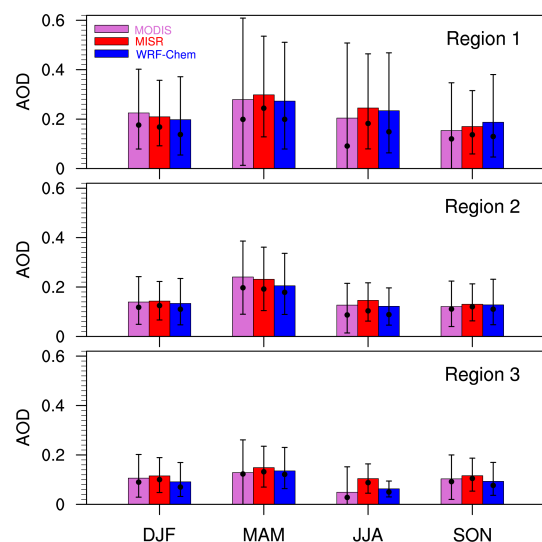


Figure 5. Seasonal mean 550 nm AOD from the MISR and MODIS retrievals, and the corresponding WRF-Chem simulation averaged for the period 2010–2014 over the three sub-regions shown in Fig. 4. The values of bars represent the mean. The vertical lines represent 10th and 90th percentile values, and the black dots represent the median values.

the three sub-regions is small for 2010–2014 indicated by the retrievals and simulation (not shown).

Available observations from several AERONET sites (Fig. 1) over East Asia, the Pacific, and the western USA are also compared with the model simulation. Figure 6 shows the comparison of observed and simulated AOD at three representative AERONET sites for 2010–2014 over East Asia, an island of the Pacific, and the western US coast. The observations and simulation agree well at all three sites, and both

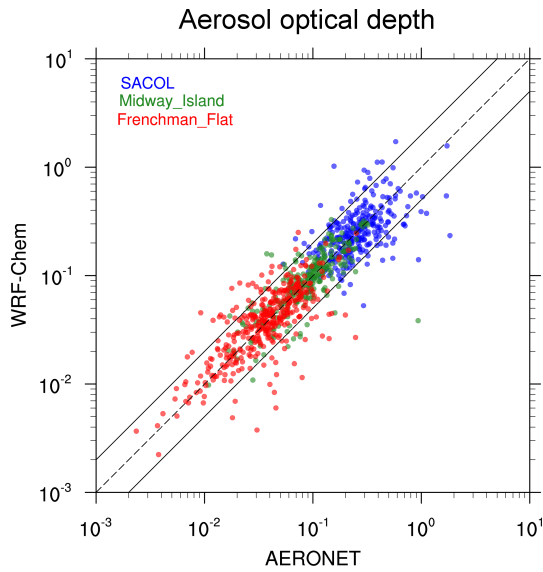


Figure 6. The AERONET observations of daily AOD at 550 nm at the three sites (SACOL, Midway Island, and Frenchman Flat) vs. the corresponding WRF-Chem simulation for the period 2010–2014.

reflect the AOD gradient from East Asia to the western USA as shown in Fig. 4. Observed AOD is the highest with a mean value of 0.31 at the SACOL site over East Asia and reduces to 0.075 at the Midway_Island site, and 0.045 at the Frenchman_Flat site. The model reproduces exactly these values at the three sites with correlation coefficients of 0.45, 0.65, and 0.64, respectively. About 90 % of simulated AOD is within a factor of 2 of the AERONET measurements.

Figure 7 further shows the monthly variation of AOD averaged at the AERONET sites over East Asia, the Pacific island, and the western USA (as shown in Fig. 1) from the AERONET observations, MODIS and MISR retrievals, and WRF-Chem simulation. For the simulated AOD, contributions by dust, BC, OM, sulfate, and other aerosols are also shown. Over East Asia, the MISR and AERONET retrievals agree well with the annual mean of 0.37 and 0.33, respectively. Their monthly variation correlates with a coefficient of 0.8. The MODIS retrievals with the annual mean of 0.48 generally overestimate AOD against the AERONET retrievals and correlate with the AERONET retrieved monthly AOD with a coefficient of 0.67. The simulation reproduces the AERONET observed AOD variability with an annual mean of 0.38 and a monthly correlation coefficient of 0.74. Model results show that anthropogenic aerosols dominate the AOD from summer to winter, while dust can significantly contribute to the AOD in spring. Over the island of Pacific (the Midway_Island site), retrievals from AERONET, MODIS, and MISR are generally consistent with each other on annual mean with values of 0.14, 0.13, and 0.14, respectively. The MISR retrievals correlate well with the AERONET retrievals in monthly variation with a coefficient of 0.70,

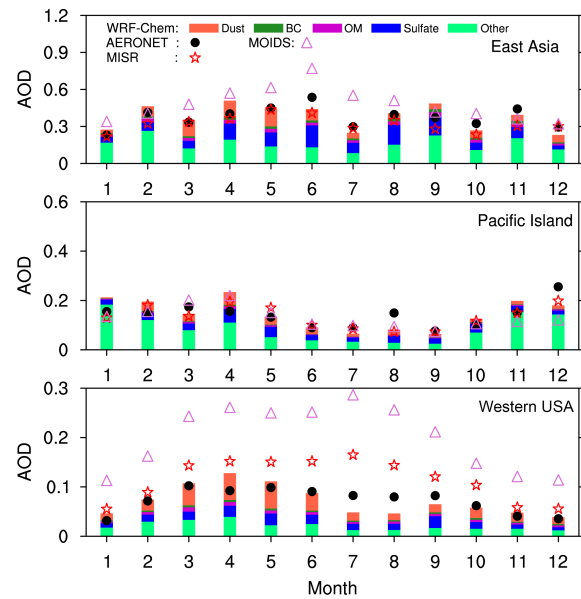


Figure 7. Monthly mean 550 nm AOD from AERONET (black dots), MODIS (purple triangles), MISR (red five-pointed stars) and the corresponding WRF-Chem simulation (histogram) averaged for the period 2010–2014 at the eastern Asian, the Pacific island, and the western USA sites as shown in Fig. 1.

which is 0.42 for MODIS, showing a minimum in summer months. The simulated annual mean AOD of 0.14 well reproduces the AERONET retrieval. The model also captures the AERONET retrieved monthly variation of AOD with a correlation coefficient of 0.64. The simulation shows that this monthly variation is largely determined by the variation of sea-salt aerosol (e.g., Smirnov et al., 2003) and Asian pollutant outflow. The trans-Pacific transported aerosols (other than sea-salt) show strong monthly variation with a maximum in April and a minimum in July. Over the western USA, the MISR and MODIS retrievals well capture the monthly variation of AERONET retrievals with correlation coefficients of ~ 0.9 , but MISR and MODIS retrieve an annual mean AOD of 0.12 and 0.20, respectively, which are higher than the AERONET retrieval of 0.07, particularly in March–October. The simulated annual mean AOD of 0.07 reproduces the AERONET retrieval. The simulation also correlates well with the AERONET retrievals with a coefficient of 0.76 in monthly variation. Both the AERONET retrieval and simulation show that the largest AOD occurs in the spring months, which has significant contribution from the dust aerosol transported across the Pacific (to be discussed in Sect. 4.5). The simulation compares more consistently with the AERONET retrieval than with the MISR and MODIS retrievals in terms of magnitude, which suggests that the difference between the MODIS and MISR retrievals and the simulation over the western USA shown in Fig. 4 is largely due to uncertainties associated with the satellite retrievals. The simulation underestimates the AERONET retrieved AOD in

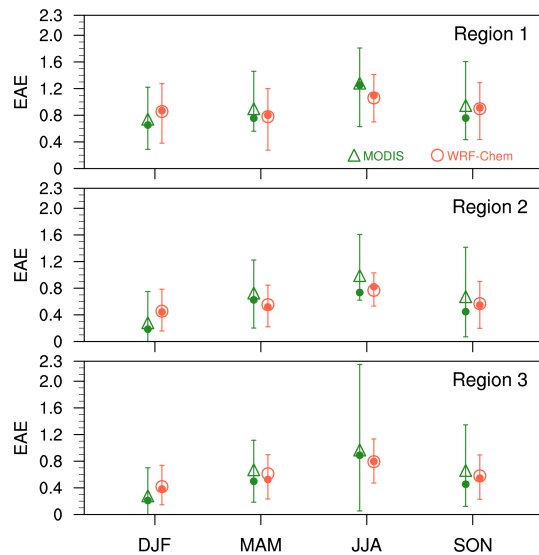


Figure 8. Seasonal mean EAE from the MODIS retrievals and the corresponding WRF-Chem simulation averaged for the period 2010–2014 over the three sub-regions shown in Fig. 4. The vertical bars represent 10th and 90th percentile values, the filled dots represent the median values, and the triangles and circles represent the mean values.

July–September. This underestimation may come from the model significant negative biases in carbonaceous aerosols in the warm season (to be discussed in Sect. 4.5).

4.2.2 Wavelength dependence

The wavelength dependence of AOD that can be represented by the EAE is an indicator of aerosol particle size (Ångström, 1929; Schuster et al., 2006). In general, relatively small values of EAE indicate that aerosol size distributions are dominated by coarse aerosols typically associated with dust and sea-salt, while relatively large values of EAE indicate fine aerosols usually contributed by anthropogenic pollution and biomass burning. Figure 8 shows the seasonal mean EAE averaged for 2010–2014 from the MODIS retrievals and the WRF-Chem simulation over the three sub-regions. The retrievals show clearly that the seasonal median EAE values peak at 1.25, 0.74, and 0.89 in JJA and reach a minimum of 0.68, 0.20, and 0.21 in DJF in three sub-regions of the western, central, and eastern Pacific, respectively. This seasonality reflects the fact that photochemistry is most active in JJA to produce fine aerosol particles such as sulfate. In general, the simulation successfully reproduces the observed EAE seasonality with the JJA maximum of 1.09, 0.82, and 0.79 and the DJF minimum of 0.83, 0.42, and 0.35 in the three sub-regions, respectively. The retrievals and simulation also show that the values of EAE are greater in the western Pacific than in the central and eastern Pacific. This pattern may reflect the dominance of the Asian pollutant outflow on the aerosol size distributions over the western Pacific, while

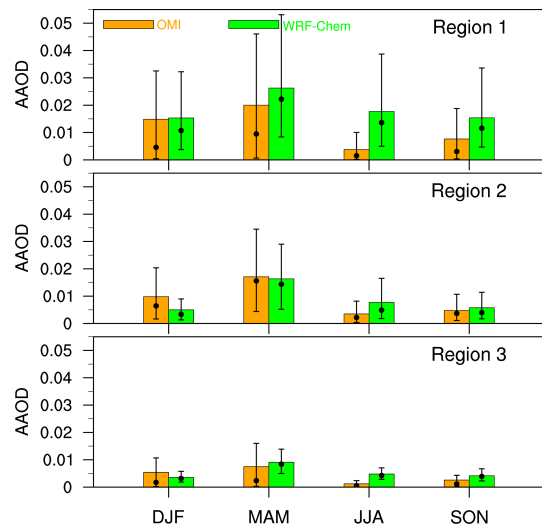


Figure 9. Seasonal mean AAOD at 500 nm from the OMI retrievals and the corresponding WRF-Chem simulation averaged for the period 2010–2014 over the three sub-regions shown in Fig. 4. The values of bars represent the mean. The vertical lines represent 10th and 90th percentile values, and the black dots represent the median values.

the relatively large-size particles of sea-salt dominates in the other two regions. Again, the annual variability of EAE over the three sub-regions is small (not shown).

4.3 Aerosol absorption optical depth

Light absorbing aerosols such as BC and dust play an important role in the atmosphere to absorb radiation and change the heating profiles in the atmosphere. AAOD is an important parameter for evaluating the model performance in simulating light absorbing aerosols. Figure 9 shows the seasonal mean AAOD at 500 nm averaged for 2010–2014 and over the three sub-regions from the OMI retrieval and the WRF-Chem simulation. The model simulated AAOD at 600 and 400 nm are used to derive the AAOD at 500 nm (using the Ångström exponent). Both retrievals and simulation show small interannual variability (not shown). The simulated seasonal mean AAOD of 0.015 over the western Pacific agrees reasonably well with the OMI retrieval of 0.014 in DJF but is higher in the other three seasons, with the largest difference in JJA. The significantly lower AAOD in seasons other than DJF from the OMI retrieval is also shown in the comparison with the AERONET retrieval (to be discussed with Fig. 10). Over the central Pacific, the simulated seasonal mean AAOD of 0.014 and 0.006 in MAM and SON, respectively, generally reproduces the retrieved AAOD of 0.017 and 0.005, but the model overestimates (underestimates) the retrieved values in JJA (DJF) with 0.008 (0.005) from the simulation and 0.004 (0.009) from the retrieval. This difference may reflect the model deficiency in simulating Asian BC outflow over the Pacific in JJA and DJF, but may also result from re-

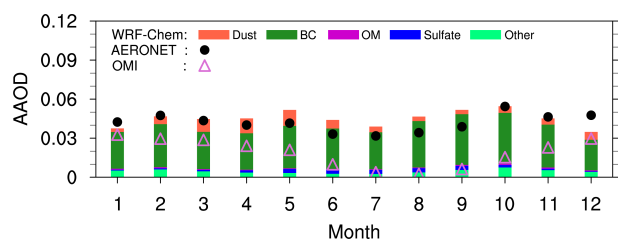


Figure 10. Monthly AAOD from the retrievals of AERONET and OMI and the corresponding WRF-Chem simulation averaged for the period 2010–2014 over the East Asia sites as shown in Fig. 1.

trieval uncertainties. The OMI retrievals may have difficulty in distinguishing the ocean color effects from those of low aerosol concentrations in the UV spectral range and ignoring the less-sufficient amounts of absorbing aerosols (Veihelmann et al., 2007; Torres et al., 2013). Jethva et al. (2014) found that the most important source of uncertainty in OMI AAOD is the effect of sub-pixel cloud contamination related to the sensor's coarse spatial resolution, which causes AAOD underestimations for cases of low aerosol load. Over the eastern Pacific, the simulated seasonal mean AAOD of 0.0035, 0.0091, 0.0048, and 0.0042 for DJF, MAM, JJA, and SON, respectively, are generally consistent with the retrieved values of 0.005, 0.007, 0.0012, and 0.003, which show the maximum value in MAM. The most significant difference occurs in JJA. Similar to over the central Pacific, the underestimation of retrieved AAOD over the clean region may contribute to the difference. The retrievals and simulation show large variability of AAOD, and they generally agree within the 10th and 90th percentiles of each other. AAOD is larger over the western Pacific than the central and eastern Pacific, which is consistent with the AOD pattern. The simulation shows that AAOD peaks in MAM followed by JJA over the three sub-regions, which may be due to the stronger outflow of dust and anthropogenic pollutants in the two seasons.

The AERONET retrieval products (version 2) also provide AAOD values but only at the sites and time when the total AOD exceeds a threshold value of 0.4 at 440 nm because the AERONET inversion algorithms require a high signal-to-noise ratio to retrieve some optical products such as AAOD. The total AOD values over the central Pacific and the western USA are less than this threshold value most of the time, and only AAOD values retrieved at the eastern Asian sites are available and reliable. Figure 10 shows the monthly variation of AAOD averaged at the AERONET sites over East Asia (Fig. 1) from the AERONET observation, OMI retrieval, and WRF-Chem simulation. The AERONET retrieval shows the monthly variation of AAOD over East Asia with relatively lower values in JJA probably due to wet removal of aerosols by precipitation and mixing with clean marine air during the eastern Asian summer monsoon (Zhao et al., 2010b). The simulation generally captures the observed monthly variability with the minimum AAOD of 0.035 and 0.032 in July from

the simulation and the AERONET retrieval, respectively, and the maximum of 0.055 and 0.054 in October. The model overestimates AAOD in the warm months (May–September) with the mean values of 0.046 and 0.036 from the simulation and retrieval, respectively, and underestimates AAOD in December and January with the mean values of 0.037 and 0.043, respectively. The model positive (negative) biases in AAOD in the warm (cold) months may be partly related to the constant anthropogenic BC emissions applied throughout the seasons, but previous studies have shown that anthropogenic BC emissions over China may have seasonal variation, with roughly 6 vs. 13 % of the annual total BC emission in summer and winter, respectively, estimated in Lu et al. (2011). The simulation shows that AAOD over East Asia is dominated by BC and is partly contributed by dust. Other aerosols contribute to a small amount of AAOD due to the internal mixing of aerosols in the atmosphere (Zhao et al., 2013a). The OMI retrieved AAOD is lower than that from AERONET and WRF-Chem, particularly in JJA and SON. The lower OMI AAOD over East Asia may also indicate its negative biases over the western Pacific (Fig. 9), where the air is significantly affected by the eastern Asian outflow. The biases in the OMI algorithm of retrieving SSA over East Asia may be also applied over the western Pacific.

4.4 Aerosol vertical distributions

Column integrated properties of aerosol (e.g., AOD and AAOD) provide useful information with regard to atmospheric aerosol loading but little information on the vertical distribution of aerosols. Previous studies have found that simulated aerosol vertical distributions differ significantly, which can affect the assessments of aerosol impacts on climate and air quality (e.g., Schulz et al., 2006; Textor et al., 2006). CALIPSO with its unique capability provides an opportunity to assess model simulation of aerosol vertical distributions (e.g., Huang et al., 2013). Figure 11 shows the vertical distributions of annual mean aerosol extinction coefficients for 2010–2014 averaged over the three sub-regions from the CALIPSO retrieval and the corresponding WRF-Chem simulation under cloud-free conditions. The model results are sampled for averaging at the locations and times where and when retrievals are available. The CALIPSO retrieval shows clearly that aerosol extinction coefficients peak near several hundred meters above the surface and then decrease with the altitude over the three sub-regions. The extinction coefficients reduce from the western to eastern Pacific. The model generally reproduces the aerosol extinction vertical variation with correlation coefficients of 0.95–0.97. The simulated aerosol extinction coefficients are consistent with the retrievals around 0.5–1 km with difference within 15 %. The difference increases in the free troposphere and below 0.5 km. The simulation is higher than the retrieval in the free troposphere (e.g., about a factor of 2 around 4 km), which may be due to the reduced sensitivity of CALIPSO

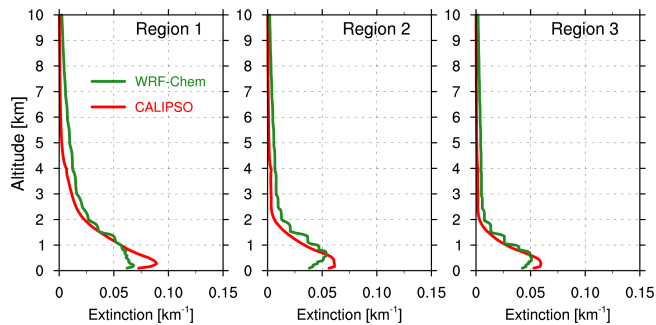


Figure 11. Vertical distributions of annual mean extinction from the CALIPSO retrieval and the corresponding WRF-Chem simulation averaged for the period 2010–2014 over the three sub-regions shown in Fig. 4.

to tenuous aerosol layers above 4 km (Yu et al., 2010). The lower (up to 30 % lower) simulated extinction coefficients below 0.5 km in all three sub-regions may indicate negative biases in estimating marine aerosol emissions and excessive wet scavenging of the model, as shown in Fig. 4. The in situ measurements over the region are needed for further validating both remote sensing data and the simulation. The simulated mass fraction of each aerosol component (Fig. 12) shows that below 1 km, sea-salt dominates the total aerosol mass over the central and eastern Pacific, while the outflow of anthropogenic aerosols and dust also makes significant contributions over the western Pacific. Above 4 km, dust is the dominant aerosol over all three sub-regions.

The seasonal variation of aerosol extinction profiles averaged for 2010–2014 (Fig. 13) shows the spring maximum, particularly above 2 km, over all three sub-regions from both the CALIPSO retrievals and the model simulation. This is likely due to the seasonality of dust outflow over the Pacific (Fig. 14) that dominates the aerosol masses above 2 km with a peak in spring (e.g., Huang et al., 2013). The model reasonably reproduces the retrieved aerosol extinction vertical variation through the seasons over the three sub-regions with the correlation coefficients of 0.93–0.98. Over the western Pacific, the simulation has larger negative biases (up to 35 %) below 1 km in DJF when sea salt has a relatively larger contribution near the surface (Fig. 14) than other seasons (up to 15–25 %), and has positive biases above 1 km. At 1–4 km, the simulated aerosol extinction is higher (up to a factor of 2) than the retrieval and the difference increases with the altitude. The comparison between the simulation and retrieval at 1–4 km is the best in DJF with the difference within 15 %. In JJA, the aerosol mass has the largest contribution from the anthropogenic pollutant outflow among the seasons with a peak at ~ 2 km above the surface. Over the central and eastern Pacific, the model has smaller negative biases (up to 20 %) below 1 km than over the western Pacific and the maximum negative bias is in DJF. Over these two regions, the seasonality of the vertical shape of each aerosol component

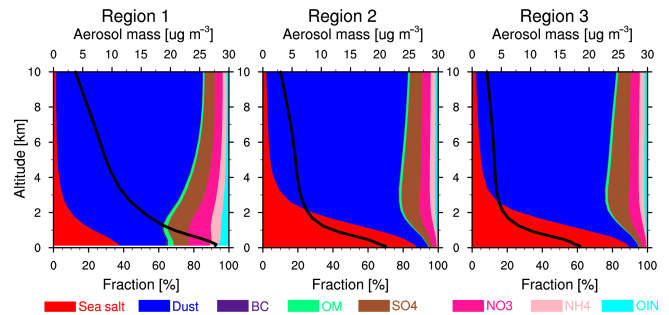


Figure 12. Vertical distributions of annual mean aerosol mass (black solid line; upper x axis) and its composition fractions (colored shade-contour; lower x axis) from the WRF-Chem simulation averaged for the period 2010–2014 over three sub-regions as shown in Fig. 4.

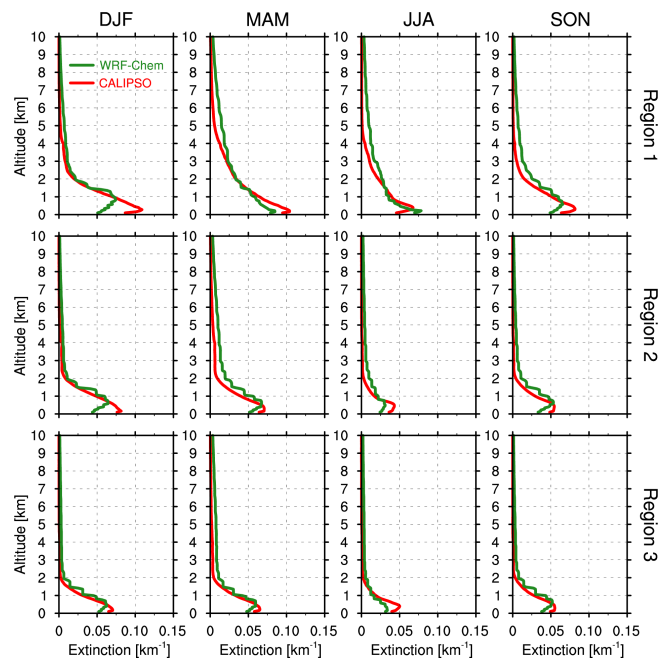


Figure 13. Vertical distributions of seasonal mean aerosol extinction from the CALIPSO retrieval and the corresponding WRF-Chem simulation averaged for the period 2010–2014 over three sub-regions as shown in Fig. 4.

contribution is similar to that over the western Pacific, except that the sea-salt contribution is larger near the surface (Fig. 14).

4.5 Aerosol surface mass concentrations over the western USA

For lack of in situ observations of aerosol masses over the Pacific, measurements of surface fine aerosol ($PM_{2.5}$) component mass concentrations from the IMPROVE network over the western USA were widely used for model evaluation of trans-Pacific transport (e.g., Chin et al., 2007; Hadley et al.,

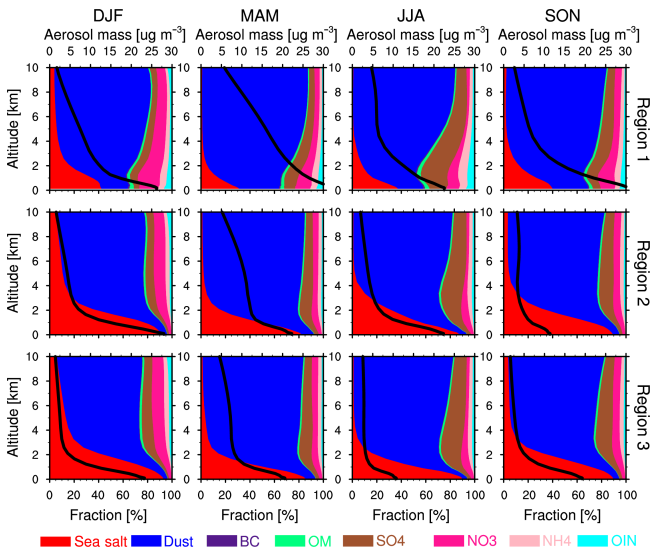


Figure 14. Vertical distributions of seasonal mean aerosol mass (black solid line; upper x axis) and its composition fraction (colored shade-contour; lower x axis) from the WRF-Chem simulation averaged for the period 2010–2014 over three sub-regions as shown in Fig. 4.

2007). Daily variation of surface fine aerosols (dust, sulfate, nitrate, BC, and OM) averaged for 2010–2014 from the IMPROVE measurements and the monthly mean of measurements and corresponding model simulation are illustrated in Fig. 15. The IMPROVE sites over the western USA (Fig. 1) that have measurements for the entire 5 years (2010–2014) and with less noisy values are divided at 40° N into two groups to represent the northwestern and southwestern USA. The averaged values over the northwestern and southwestern sites are shown.

At both northwestern and southwestern sites, the model generally captures the observed monthly variation of dust with the correlation coefficients of 0.61 and 0.55, respectively. Both the observation and simulation show the maximum dust mass concentration in MAM and the minimum in DJF. The model simulates higher annual mean surface dust concentrations (0.25 and $0.56 \mu\text{g m}^{-3}$ over the northwestern and southwestern, respectively) than the observation (0.18 and $0.35 \mu\text{g m}^{-3}$, respectively). The observed surface sulfate concentrations are the lowest in the cold season (0.17 and $0.18 \mu\text{g m}^{-3}$ in DJF over the northwestern and southwestern, respectively) when photochemistry is least active, and the highest in the warm season (0.47 and $0.63 \mu\text{g m}^{-3}$ in June–September (JJAS), respectively) when the most active photochemistry occurs. This seasonality of sulfate may also be contributed by the seasonality of wet removal (much more precipitation in DJF). Over the northwestern and southwestern, the simulation generally reproduces the magnitude and seasonality of sulfate with the minimum surface concentrations of 0.17 and $0.25 \mu\text{g m}^{-3}$, respectively, in DJF and the

maximum surface concentrations of 0.49 and $0.62 \mu\text{g m}^{-3}$, respectively, in JJAS, and monthly correlation coefficients of 0.78 and 0.83 , respectively. Nitrate shows a seasonality that is opposite to that of sulfate, with a maximum surface concentration occurring in the cold season (0.72 and $1.22 \mu\text{g m}^{-3}$ in December–January over the northwestern and southwestern, respectively) and a minimum in the warm season (0.25 and $0.35 \mu\text{g m}^{-3}$ in JJA, respectively), which can be explained by the combined effects of temperature and vertical turbulent mixing (Zhao et al., 2013a). The simulation generally reproduces the seasonality of nitrate with a monthly correlation coefficient of 0.75 and 0.83 over the northwestern and southwestern, respectively. Over the northwestern and southwestern, the model simulates reasonably the maximum surface nitrate concentration of 0.69 and $1.35 \mu\text{g m}^{-3}$, respectively, in the cold season and the minimum with values of 0.18 and $0.42 \mu\text{g m}^{-3}$, respectively, in the warm season. The simulation has relatively larger positive biases (a factor of 2) in months (February, March, October, and November) between the cold and warm seasons, which may reflect the model deficiency in aerosol thermodynamics (i.e., the partitioning of nitrate aerosol to the gas phase in these months is too slow in the model). In general, both observation and simulation show higher surface dust, sulfate, and nitrate concentrations over the southwestern than the northwestern.

A sensitivity simulation without dust, fire, and anthropogenic emissions over North America (10 – 70° N and 170 – 60° W) indicates that the trans-Pacific transported dust dominates the total dust amount in all seasons at the northern and southern sites with the contribution of 80 and 60% , respectively, on annual mean, particularly in MAM with the contribution of >90 and $\sim 85\%$, respectively. At the southern sites, the trans-Pacific dust makes the lowest contribution of 19% in DJF. The large contribution of trans-Pacific dust indicates that the simulated overestimation of surface dust concentrations may result from the excessive trans-Pacific transport of dust, which is also indicated in the comparison with the CALIPSO retrieval that shows the simulated aerosol extinction is overestimated above 1 km over the North Pacific. The difference may also be partly from the observation uncertainties. As described in Sect. 3.2.2, the mass of soil dust is calculated from a linear combination of the measured elements associated predominantly with soil, including Al, Si, Ca, Fe, and Ti. The uncertainties associated with the reported dust values reflect the range and variation of mineral composition from a variety of soil types. The sensitivity simulation also shows that trans-Pacific transported sulfate can make significant contribution to its surface concentration over the western USA, and the relative contributions are larger when the surface concentrations are lower with $\sim 60\%$ in DJF averaged at all sites and $\sim 35\%$ in JJA. The trans-Pacific nitrate contributes a relatively small amount ($\sim 15\%$) to the total nitrate surface concentration.

There is a significant difference in BC and OM surface concentrations between the observations and simulation. At

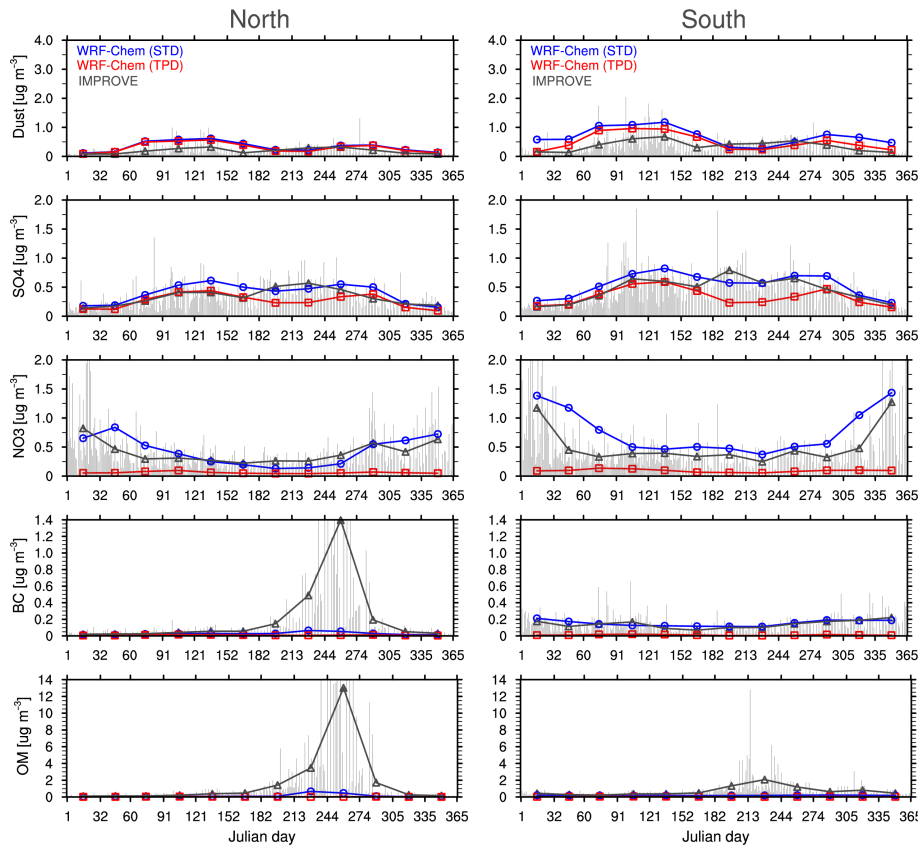


Figure 15. Daily mass concentrations of fine-mode ($\text{PM}_{2.5}$) dust, sulfate, nitrate, BC, and OM averaged for the period 2010–2014 at the IMPROVE sites over the northwestern and southwestern USA (shown in Fig. 1) from the IMPROVE observation (vertical gray bars) and the monthly average of the IMPROVE observation (gray triangles) and the corresponding WRF-Chem standard simulation (STD; blue dots) and the sensitivity simulation without North American emissions (TPD; red dots).

the northwestern sites, the observed BC and OM show significant seasonal variation with the highest surface concentration in JJAS. The sensitivity simulation shows that the peak is dominated by the North American emission that is contributed by biomass burning with a maximum in JJAS (Chin et al., 2007). The simulation captures this seasonality to some extent with monthly correlation coefficients of 0.74 and 0.69 for BC and OM, respectively. However, the simulation significantly underestimates the JJAS peak with 0.05 and $0.49 \mu\text{g m}^{-3}$ BC and 0.5 and $4.5 \mu\text{g m}^{-3}$ OM from the simulation and observation, respectively. These significant negative biases in the model are likely from uncertainties in the GFEDv3 biomass burning inventory for the simulation period. The monthly mean emissions at a relatively coarse horizontal resolution may not be able to capture the strong local fire events. Mao et al. (2011) pointed out that the GFED inventory may underestimate the magnitude of biomass burning emissions in the western USA due to the issue of detecting small fires, for example, from prescribed and agricultural burning (e.g., Randerson et al., 2012; Giglio et al., 2010). Mao et al. (2014) estimated that the biomass burning BC emissions inverted from the IMPROVE observa-

tions can be a factor of 5 higher than the GFED inventory in July–September over the Western USA. Another biomass burning emission inventory FINN (Fire INventory from the National Center for Atmospheric Research, NCAR) (Wiedinmyer et al., 2011) also shows a factor of 3 higher BC emissions than the GFED inventory over the northwestern USA (100 – 125° W and 40 – 50° N) in September 2011 (not shown).

At the southwestern sites, the impact of biomass burning on the BC and OM surface concentrations seems relatively small. The observations show the maximum BC surface concentration of $0.17 \mu\text{g m}^{-3}$ in DJF and the minimum of $0.09 \mu\text{g m}^{-3}$ in JJA, which is likely due to stronger vertical turbulent mixing in JJA compared with DJF (Zhao et al., 2013a). The simulation can well capture the magnitude and seasonality of surface BC concentration with the monthly correlation coefficient of 0.78 and the maximum of $0.19 \mu\text{g m}^{-3}$ in DJF and the minimum of $0.10 \mu\text{g m}^{-3}$ in JJA. The observed OM still shows the peak concentration of $1.27 \mu\text{g m}^{-3}$ in JJA, and the model significantly underestimates the peak OM concentration with a value of $0.20 \mu\text{g m}^{-3}$. The negative bias of OM over the southwestern seems not to be related to the underestimation of biomass

burning because BC is reasonably simulated. This seasonal variability may be determined by the secondary production of OM, which peaks in JJA because photochemistry is more active and emissions of biogenic volatile organic compounds are higher in the warm season. The underestimation of secondary organic aerosol (SOA) may be due to the uncertainty of biogenic emissions (Zhao et al., 2016) and the outdated SOA mechanism used in the current version of WRF-Chem (Shrivastava et al., 2011). Besides the emission and model deficiency, another source of the difference between the simulation and observation may be from the sub-grid variability of emissions and surface concentrations that confounds the comparison of model simulation at 1-degree horizontal grid resolution and the point measurements from the individual sites. On the other hand, it is also noteworthy that uncertainties in the IMPROVE carbonaceous aerosol data are also relatively high because they are inferred from optical/thermal measurements. The sensitivity simulation again shows that the peaks of BC and OM surface concentrations are dominated by the North American emissions.

5 Summary and conclusion

A fully coupled meteorology-chemistry model (WRF-Chem) has been configured to conduct quasi-global simulation for 5 years (2010–2014). The simulation results are evaluated for the first time with various reanalysis and observational data sets, including precipitation from GPCP, wind fields from MERRA, AOD, EAE, and AAOD from MODIS, MISR, OMI, and AERONET, aerosol extinction profiles from CALIPSO, and aerosol surface mass concentrations from IMPROVE. In this study, the evaluation and analysis focus on the trans-Pacific transport region for the purpose of demonstrating the capability of using the quasi-global WRF-Chem simulation to provide consistent lateral chemical boundaries for nested regional WRF-Chem simulations that can be used to investigate the impact of trans-Pacific transported aerosols on the regional air quality and climate over the western USA. The main conclusion is summarized below:

- The comparison of simulated AOD with the satellite and AERONET retrievals reveals that the model can well capture the spatial gradient of aerosol mass loading, decreasing from the western to eastern Pacific, resulting from the sea-salt loading and the Asian pollutant outflow. The seasonal variation of aerosols across the Pacific with the maximum AOD in MAM is also reproduced by the model. The model underestimates AOD over the ocean to the south of 20° N and over the continent of North America against the satellite retrievals. This discrepancy may reflect the model underestimation of marine emissions and/or overestimation of aerosol wet removal or the positive retrieval errors due to cloud contamination. Compared with the AERONET

retrieval, the difference of AOD over the western USA between the simulation and satellite retrievals may be due to the uncertainty in the satellite retrievals over the continent.

- The assessment of simulated EAE indicates that the model generally captures the observed smaller-size aerosols over the western Pacific contributed by the Asian pollutant outflow compared to the relatively larger particles over the central and eastern Pacific with more contributions from sea salt. The model also simulates the consistent seasonality of EAE with observations showing a minimum in DJF and a maximum in JJA due to the active production of small particles in warm seasons.
- The model reasonably simulates the decreasing gradient of OMI derived AAOD from the eastern to western of Pacific. The simulation shows a peak of AAOD in MAM due to the strong outflow of dust and anthropogenic pollutants. The comparison with AERONET retrieved AAOD over East Asia may indicate that the OMI SSA retrieval has positive biases over East Asia and also the western Pacific, particularly in JJA. Over East Asia, the model positive (negative) biases in AAOD in the warm (cold) months may be partly due to the neglect of the seasonal variability of anthropogenic BC emissions in this study.
- The model generally captures the CALIPSO retrieved vertical gradient of aerosol extinction coefficients roughly decreasing with the altitude over the Pacific. Near the surface, the model biases in estimating marine aerosol emissions may contribute to the discrepancy between the simulation and retrievals. The difference between the simulation and retrievals in the free troposphere may be due to the reduced sensitivity of CALIPSO to the aerosol layers above 4 km. The model well captures the seasonality of aerosol extinction profiles with a maximum in MAM, which is largely controlled by the activity of dust outflow events over the Pacific.
- Compared with the measurements from the IMPROVE sites over the western USA, the model simulates reasonable magnitudes and seasonality of the observed sulfate and nitrate surface concentrations with peaks in JJA and DJF, respectively. The simulation has relatively larger positive biases of nitrate surface concentrations in early spring and late fall, which may reflect the model deficiency in aerosol thermodynamics that the partitioning of nitrate aerosol to the gas phase in these months is too slow in the model. The simulation captures the observed seasonality of dust surface concentrations with the maximum and minimum in MAM and DJF, respectively, but

generally overestimates the observed dust surface concentrations, which may be due to the excessive trans-Pacific dust. The difference may also be partly from the observation uncertainties. Over the southwestern USA, the simulation reproduces the magnitude and seasonality of surface BC concentrations that show the maximum in DJF, but significant underestimates the surface OM concentrations in JJA likely due to the negative biases in SOA production. Over the northwestern USA, the simulation significantly underestimates surface BC and OM concentrations likely due to the uncertainties in fire emissions that may not capture the strong local fire events. Another source of the difference may be due to the discrepancy in spatial scales between site observations and model outputs for the grid cell area of 1-degree resolution. In addition, uncertainties in IMPROVE may also contribute to the discrepancy, in particular for carbonaceous aerosols that are inferred from optical/thermal measurements.

- The sensitivity simulation shows that the trans-Pacific transported dust dominates the dust surface concentrations in the western USA, particularly in MAM. The trans-Pacific transported sulfate and nitrate can also make significant contribution to their surface concentrations over the rural areas of the western USA. The peaks of BC and OM surface concentrations over the western USA are dominated by the North American emissions. These sensitivity simulation results may be different to some extent from other models (e.g., Chin et al., 2007), which could result from the considerable differences in aerosol composition and vertical distributions due to differences in model treatments of emissions and removal processes as revealed by several inter-comparison studies (Barrie et al., 2001; Penner et al., 2002; Textor et al., 2006). More detailed model inter-comparison of the trans-Pacific transport of aerosols deserves further study.

Although dust and biomass burning emissions in general have considerable year-to-year variations, the interannual variability of seasonal AOD for 2010–2014 average over the three sub-regions of the Pacific is small as indicated by the retrievals and simulation. It is noteworthy that the trans-Pacific aerosols identified in this study include not only the outflow of Asian pollutants and dust but also European pollutants and African dust that are transported to Asia and then merged with the Asian outflow. This has been recognized by previous studies (e.g., Chin et al., 2007). The evaluation in this study successfully demonstrates that the WRF-Chem quasi-global simulation with some improvements in emission inventories can be used for studying trans-Pacific transport of aerosols and providing reasonable inflow chemical boundaries for the western USA to further understand the impact of transported pollutants on the air quality and regional climate with high-resolution nested regional modeling. It needs to be noted

that the aerosol optical properties, such as AOD, AAOD, and EAE, derived from the retrievals and simulation have some different assumptions of the physical and optical parameters; therefore, the link between the model and the satellite data are only qualitative or semi-quantitative. Evaluation of model results with in situ observations would be informative. In situ data even for specific events are valuable especially over Asia and the Pacific where public data are currently sparse or inaccessible, although some observations may be obtained through collaborations. Last but not least, the model biases against observations may also be partly contributed by the uncertainties in emissions. Some recently updated anthropogenic emissions (e.g., Janssens-Maenhout et al., 2015; Li et al., 2015) and other biomass burning emissions with higher temporal and spatial resolutions (e.g., Wiedinmyer et al., 2011) may be used in future studies to investigate the impact of emission uncertainties on trans-Pacific aerosols over the western USA.

Code availability

The WRF-Chem version 3.5.1 release can be obtained at http://www2.mmm.ucar.edu/wrf/users/download/get_source.html. A general WRF-Chem user's guide is also available online (<http://ruc.noaa.gov/wrf/WG11/>). Code modifications include changes to the chemical boundary treatment using periodic boundary conditions in the zonal direction for quasi-global WRF-Chem simulation. Other changes to the model include the oceanic (sea salt and dimethyl sulfide) emission schemes and the convective transport and removal scheme of tracers that play a significant role in quasi-global WRF-Chem simulations of aerosols. These modifications and model configuration for conducting quasi-global WRF-Chem simulations here are available upon request by contacting the corresponding author and will be incorporated in the future available release of WRF-Chem.

Data availability

The RETRO global anthropogenic emission inventory (Schultz et al., 2007) can be obtained through the link below: ftp://aftp.fsl.noaa.gov/divisions/taq/global_emissions/global_emissions_v3_24aug2015.tar.gz. The IMPROVE observations (Hand et al., 2011) is available through the link below: <http://views.cira.colostate.edu/fed/DataWizard/Default.aspx>.

Acknowledgements. This research was supported by the Office of Science of the U.S. Department of Energy (DOE) as part of the Regional & Global Climate Modeling (RGCM) program. Jianping Huang acknowledges support from the National Basic Research Program of China (2012CB955301). Hongbin Yu was supported by NASA CALIPSO project (NNX14AB21G) managed by David Considine. This study used computing resources from

the PNNL Institutional Computing. Pacific Northwest National Laboratory is operated by Battelle Memorial Institute for the DOE under contract DE-AC05-76RL01830. The CALIPSO data were obtained from the NASA Langley Research Center Atmospheric Sciences Data Center. MODIS and MISR data were obtained from the NASA Atmospheric Science Data Center. OMI data were obtained from the NASA Goddard Earth Sciences Data and Information Services Center.

Edited by: J. Williams

References

- Ahn, C., Torres, O., and Bhartia, P. K.: Comparison of Ozone Monitoring Instrument UV Aerosol Products with Aqua/Moderate Resolution Imaging Spectroradiometer and Multiangle Imaging Spectroradiometer observations in 2006, *J. Geophys. Res.*, 113, D16S27, doi:10.1029/2007JD008832, 2008.
- Alizadeh-Choobari, O., Zawar-Reza, P., and Sturman, A.: The global distribution of mineral dust and its impacts on the climate system: A review, *Atmos. Res.*, 138, 152–165, doi:10.1016/j.atmosres.2013.11.007, 2014.
- Alizadeh-Choobari, O., Sturman, A. P., and Zawar-Reza, P.: Global distribution of mineral dust and its impact on radiative fluxes as simulated by WRF-Chem, *Meteorol. Atmos. Phys.*, 127, 635–648, doi:10.1007/s00703-015-0390-4, 2015.
- Anderson, T. L., Wu, Y., Chu, D. A., Schmid, B., Redemann, J., and Dubovik, O.: Testing the MODIS satellite retrieval of aerosol fine-mode fraction, *J. Geophys. Res.*, 110, D18204, doi:10.1029/2005JD005978, 2005.
- Ångström, A.: On the atmospheric transmission of Sun radiation and on dust in the air, *Geogr. Ann.*, 11, 156–166, 1929.
- Ault, A. P., Williams, C. R., White, A. B., Neiman, P. J., Creamean, J. M., Gaston, C. J., Ralph, F. M., and Prather, K. A.: Detection of Asian dust in California orographic precipitation, *J. Geophys. Res.*, 116, D16205, doi:10.1029/2010JD015351, 2011.
- Barnard, J. C., Fast, J. D., Paredes-Miranda, G., Arnott, W. P., and Laskin, A.: Technical Note: Evaluation of the WRF-Chem “Aerosol Chemical to Aerosol Optical Properties” Module using data from the MILAGRO campaign, *Atmos. Chem. Phys.*, 10, 7325–7340, doi:10.5194/acp-10-7325-2010, 2010.
- Barrie, L. A., Yi, Y., Leaitch, W. R., Lohmann, U., Kasibhatla, P., Roelofs, G. J., Wilson, J., McGovern, F., Benkovitz, C., Melieres, M. A., Law, K., Prospero, J., Kritiz, M., Bergmann, D., Bridgeman, C., Chin, M., Christensen, J., Easter, R., Feichter, J., Land, C., Jeuken, A., Kjellstrom, E., Koch, D., and Rasch, P.: A comparison of large-scale atmospheric sulphate aerosol models (COSAM): overview and highlights, *Tellus*, 53B, 615–645, 2001.
- Binkowski, F. S. and Shankar, U.: The Regional Particulate Matter Model 1. Model description and preliminary results, *J. Geophys. Res.*, 100, 26191–26209, 1995.
- Chapman, E. G., Gustafson Jr., W. I., Easter, R. C., Barnard, J. C., Ghan, S. J., Pekour, M. S., and Fast, J. D.: Coupling aerosol-cloud-radiative processes in the WRF-Chem model: Investigating the radiative impact of elevated point sources, *Atmos. Chem. Phys.*, 9, 945–964, doi:10.5194/acp-9-945-2009, 2009.
- Chen, S., Huang, J., Zhao, C., Qian, Y., Leung, L. R., and Yang, B.: Modeling the transport and radiative forcing of Taklimakan dust over the Tibetan Plateau: A case study in the summer of 2006, *J. Geophys. Res.*, 118, 797–812, doi:10.1002/jgrd.50122, 2013.
- Chen, S., Zhao, C., Qian, Y., Leung, L. R., Huang, J., Huang, Z., Bi, J., Zhang, W., Shi, J., Yang, L., Li, D., and Li, J.: Regional modeling of dust mass balance and radiative forcing over East Asia using WRF-Chem, *Aeolian Research*, 15, 15–30, doi:10.1016/j.aeolia.2014.02.001, 2014.
- Chin, M., Chu, A., Levy, R., Remer, L., Kaufman, Y., Holben, B., Eck, T., Ginoux, P., and Gao, Q.: Aerosol distribution in the Northern Hemisphere during ACE-Asia: Results from global model, satellite observations, and Sun photometer measurements, *J. Geophys. Res.*, 109, D23S90, doi:10.1029/2004JD004829, 2004.
- Chin, M., Diehl, T., Ginoux, P., and Malm, W.: Intercontinental transport of pollution and dust aerosols: implications for regional air quality, *Atmos. Chem. Phys.*, 7, 5501–5517, doi:10.5194/acp-7-5501-2007, 2007.
- Chow, J. C., Chen, L.-W. A., Watson, J. G., Lowenthal, D. H., Magliano, K. A., Turkiewicz, K., and Lehman, D. E.: PM_{2.5} chemical composition and spatiotemporal variability during the California Regional PM₁₀/PM_{2.5} Air Quality Study (CRPAQS), *J. Geophys. Res.*, 111, D10S04, doi:10.1029/2005JD006457, 2006.
- Creamean, J. M., Suski, K. J., Rosenfeld, D., Cazorla, A., DeMott, P. J., Sullivan, R. C., White, A. B., Ralph, F. M., Minnis, P., Comstock, J. M., Tomlinson, J. M., and Prather, K. A.: Dust and Biological Aerosols from the Sahara and Asia Influence Precipitation in the Western US, *Science*, 339, 1572, doi:10.1126/science.1227279, 2013.
- Dentener, F., Kinne, S., Bond, T., Boucher, O., Cofala, J., Generoso, S., Ginoux, P., Gong, S., Hoelzemann, J. J., Ito, A., Marelli, L., Penner, J. E., Putaud, J.-P., Textor, C., Schulz, M., van der Werf, G. R., and Wilson, J.: Emissions of primary aerosol and precursor gases in the years 2000 and 1750 prescribed data-sets for AeroCom, *Atmos. Chem. Phys.*, 6, 4321–4344, doi:10.5194/acp-6-4321-2006, 2006.
- Diner, D. J., Beckert, J. C., Reilly, T. H., Bruegge, C. J., Conel, J. E., Kahn, R. A., Martonchik, J. V., Ackerman, T. P., Davies, R., Gerstl, S. A. W., Gordon, H. R., Muller, J. P., Myneni, R. B., Sellers, P. J., Pinty, B., and Verstraete, M. M.: Multi-angle Imaging SpectroRadiometer (MISR) Instrument Description and Experiment Overview, *IEEE T. Geosci. Remote*, 36, 1072–1087, 1998.
- Dubovik, O. and King, M. D.: A flexible inversion algorithm for retrieval of aerosol optical properties from Sun and sky radiance measurements, *J. Geophys. Res.*, 105, 20673–20696, 2000.
- Dubovik, O., Holben, B. N., Lapyonok, T., Sinyuk, A., Mishchenko, M. I., Yang, P., and Slutsker, I.: Non-spherical aerosol retrieval method employing light scattering by spheroids, *Geophys. Res. Lett.*, 29, 1415, doi:10.1029/2001GL014506, 2002.
- Easter, R. C., Ghan, S. J., Zhang, Y., Saylor, R. D., Chapman, E. G., Laulainen, N. S., Abdul-Razzak, H., Leung, L. R., Bian, X., and Zaveri, R. A.: MIRAGE: Model Description and Evaluation of Aerosols and Trace Gases, *J. Geophys. Res.*, 109, D20210, doi:10.1029/2004JD004571, 2004.
- Eck, T. F., Holben, B. N., Reid, J. S., Dubovik, O., Smirnov, A., O’Neill, N. T., Slutsker, I., and Kinn, S.: Wavelength dependence

- of the optical depth of biomass burning urban, and desert dust aerosols, *J. Geophys. Res.*, 104, 31333–31349, 1999.
- Eguchi, K., Uno, I., Yumimoto, K., Takemura, T., Shimizu, A., Sugimoto, N., and Liu, Z.: Trans-pacific dust transport: integrated analysis of NASA/CALIPSO and a global aerosol transport model, *Atmos. Chem. Phys.*, 9, 3137–3145, doi:10.5194/acp-9-3137-2009, 2009.
- Fairlie, T. D., Jacob, D. J., and Park, R. J.: The impact of transpacific transport of mineral dust in the United States, *Atmos. Environ.*, 41, 1251–1266, 2007.
- Fan, J., Leung, L. R., DeMott, P. J., Comstock, J. M., Singh, B., Rosenfeld, D., Tomlinson, J. M., White, A., Prather, K. A., Minnis, P., Ayers, J. K., and Min, Q.: Aerosol impacts on California winter clouds and precipitation during CalWater 2011: local pollution versus long-range transported dust, *Atmos. Chem. Phys.*, 14, 81–101, doi:10.5194/acp-14-81-2014, 2014.
- Fan, J., Rosenfeld, D., Yang, Y., Zhao, C., Leung, L. R., and Li, Z.: Substantial contribution of anthropogenic air pollution to catastrophic floods in Southwest China, *Geophys. Res. Lett.*, 42, 6066–6075, doi:10.1002/2015GL064479, 2015.
- Fast, J., Aiken, A. C., Allan, J., Alexander, L., Campos, T., Canagaratna, M. R., Chapman, E., DeCarlo, P. F., de Foy, B., Gaffney, J., de Gouw, J., Doran, J. C., Emmons, L., Hodzic, A., Herndon, S. C., Huey, G., Jayne, J. T., Jimenez, J. L., Kleinman, L., Kuster, W., Marley, N., Russell, L., Ochoa, C., Onasch, T. B., Pekour, M., Song, C., Ulbrich, I. M., Warneke, C., Welsh-Bon, D., Wiedinmyer, C., Worsnop, D. R., Yu, X.-Y., and Zaveri, R.: Evaluating simulated primary anthropogenic and biomass burning organic aerosols during MILAGRO: implications for assessing treatments of secondary organic aerosols, *Atmos. Chem. Phys.*, 9, 6191–6215, doi:10.5194/acp-9-6191-2009, 2009.
- Fast, J. D., Gustafson, W. I., Easter, R. C., Zaveri, R. A., Barnard, J. C., Chapman, E. G., Grell, G. A., and Peckham, S. E.: Evolution of ozone, particulates, and aerosol direct radiative forcing in the vicinity of Houston using a fully coupled meteorology-chemistry- aerosol model, *J. Geophys. Res.*, 111, D21305, doi:10.1029/2005JD006721, 2006.
- Fast, J. D., Allan, J., Bahreini, R., Craven, J., Emmons, L., Ferrare, R., Hayes, P. L., Hodzic, A., Holloway, J., Hostetler, C., Jimenez, J. L., Jonsson, H., Liu, S., Liu, Y., Metcalf, A., Middlebrook, A., Nowak, J., Pekour, M., Perring, A., Russell, L., Sedlacek, A., Seinfeld, J., Setyan, A., Shilling, J., Shrivastava, M., Springston, S., Song, C., Subramanian, R., Taylor, J. W., Vиноj, V., Yang, Q., Zaveri, R. A., and Zhang, Q.: Modeling regional aerosol and aerosol precursor variability over California and its sensitivity to emissions and long-range transport during the 2010 CalNex and CARES campaigns, *Atmos. Chem. Phys.*, 14, 10013–10060, doi:10.5194/acp-14-10013-2014, 2014.
- Fischer, E. V., Hsu, N. C., Jaffe, D. A., Jeong, M.-J., and Gong, S. L.: A decade of dust: Asian dust and springtime aerosol load in the US Pacific Northwest, *Geophys. Res. Lett.*, 36, L03821, doi:10.1029/2008GL036467, 2009.
- Fonseca, R. M., Zhang, T., and Yong, K.-T.: Improved simulation of precipitation in the tropics using a modified BMJ scheme in the WRF model, *Geosci. Model Dev.*, 8, 2915–2928, doi:10.5194/gmd-8-2915-2015, 2015.
- Forster, C., Cooper, O., Stohl, A., Eckhardt, S., James, P., Dunlea, E., Nicks, D. K., Holloway, J. S., Hubler, G., Parrish, D. D., Ryerson, T. B., and Trainer, M.: Lagrangian transport model forecasts and a transport climatology for the Intercontinental Transport and Chemical Transformation 2002 (ITCT 2K2) measurement campaign, *J. Geophys. Res.*, 109, D07S92, doi:10.1029/2003JD003589, 2004.
- Gao, Y., Liu, X., Zhao, C., and Zhang, M.: Emission controls versus meteorological conditions in determining aerosol concentrations in Beijing during the 2008 Olympic Games, *Atmos. Chem. Phys.*, 11, 12437–12451, doi:10.5194/acp-11-12437-2011, 2011.
- Gao, Y., Zhao, C., Liu, X. H., Zhang, M. G., and Leung, L. R.: WRF-Chem simulations of aerosols and anthropogenic aerosol radiative forcing in East Asia, *Atmos. Environ.*, 92, 250–266, 2014.
- Giglio, L., Randerson, J. T., van der Werf, G. R., Kasibhatla, P. S., Collatz, G. J., Morton, D. C., and DeFries, R. S.: Assessing variability and long-term trends in burned area by merging multiple satellite fire products, *Biogeosciences*, 7, 1171–1186, doi:10.5194/bg-7-1171-2010, 2010.
- Ginoux, P., Chin, M., Tegen, I., Prospero, J. M., Holben, B., Dubovik, O., and Lin, S. J.: Sources and distributions of dust aerosols simulated with the GOCART model, *J. Geophys. Res.*, 106, 20255–20273, 2001.
- Gong, S. L.: A parameterization of sea-salt aerosol source function for sub- and super-micron particles, *Global Biogeochem. Cy.*, 17, 1097, doi:10.1029/2003GB002079, 2003.
- Grell, G. A., Peckham, S. E., Schmitz, R., McKeen, S. A., Frost, G., Skamarock, W. C., and Eder, B.: Fully coupled “online” chemistry within the WRF model, *Atmos. Environ.*, 39, 6957–6957, doi:10.1016/j.atmosenv.2005.04.027, 2005.
- Guenther, A., Zimmerman, P., and Wildermuth, M.: Natural volatile organic compound emission rate estimates for US woodland landscapes, *Atmos. Environ.*, 28, 1197–1210, doi:10.1016/1352-2310(94)90297-6, 1994.
- Gustafson, W. I., Chapman, E. G., Ghan, S. J., Easter, R. C., and Fast, J. D.: Impact on modeled cloud characteristics due to simplified treatment of uniform cloud condensation nuclei during NEAQS 2004, *Geophys. Res. Lett.*, 34, L19809, doi:10.1029/2007GL030021, 2007.
- Hadley, O. L., Ramanathan, V., Carmichael, G. R., Tang, Y., Corrigan, C. E., Roberts, G. C., and Mauger, G. S.: Trans-Pacific transport of black carbon and fine aerosols ($D < 2.5 \mu\text{m}$) into North America, *J. Geophys. Res.*, 112, D05309, doi:10.1029/2006JD007632, 2007.
- Hadley, O. L., Corrigan, C. E., Kirchstetter, T. W., Cliff, S. S., and Ramanathan, V.: Measured black carbon deposition on the Sierra Nevada snow pack and implication for snow pack retreat, *Atmos. Chem. Phys.*, 10, 7505–7513, doi:10.5194/acp-10-7505-2010, 2010.
- Hagos, S. M., Feng, Z., Burleyson, C. D., Zhao, C., Martini, M. N., and Berg, L. K.: Moist Process Biases in Simulations of the Madden-Julian Oscillation Episodes Observed during the AMIE/DYNAMO Field Campaign, *J. Climate*, 29, 1091–1107, doi:10.1175/JCLI-D-15-0349.1, 2016.
- Hand, J., Copeland, S. A., Day, D. E., Dillner, A. M., Indresand, H., Malm, W. C., McDade, C. E., Moore Jr., C. T., Pitchford, M. L., Schichtel, B. A., and Watson, J. G.: Spatial and seasonal patterns and temporal variability of haze and its constituents in the United States: Report V, June 2011, available at: <http://vista.cira.colostate.edu/improve/Publications/Reports/2011/2011.htm> (last access: 2 May 2016), 2011.

- Heald, C. L., Jacob, D. J., Park, R. J., Alexander, B., Fairlie, T. D., Yantosca, R. M., and Chu, D. A.: Transpacific transport of Asian anthropogenic aerosols and its impact on surface air quality in the United States, *J. Geophys. Res.*, 111, D14310, doi:10.1029/2005JD006847, 2006.
- Hess, M., Koepke, P., and Schult, I.: Optical Properties of Aerosols and Clouds: The Software Package OPAC, *Bull. Am. Meteorol. Soc.*, 79, 831–844, 1998.
- Holben, B. N., Eck, T. F., Slutsker, I., Tanre, D., Buis, J. P., Setzer, A., Vermote, E., Reagan, J. A., Kaufman, Y. J., Nakajima, T., Lavenu, F., Jankowiak, I., and Smirnov, A.: AERONET – A Federated Instrument Network and Data Archive for Aerosol Characterization, *Remote Sens. Environ.*, 66, 1–16, 1998.
- Holben, B. N., Tanr, D., Smirnov, A., Eck, T. F., Slutsker, I., Abuhassan, N., Newcomb, W. W., Schafer, J. S., Chatenet, B., Lavenu, F., Kaufman, Y. J., Castle, J. V., Setzer, A., Markham, B., Clark, D., Frouin, R., Halthore, R., Karneli, A., O'Neill, N. T., Pietras, C., Pinker, R. T., Voss, K., and Zibordi, G.: An emerging ground-based aerosol climatology: Aerosol optical depth from AERONET, *J. Geophys. Res.*, 106, 12067–12097, 2001.
- Hsu, N. C., Tsay, S. C., King, M. D., and Herman, J. R.: Deep Blue Retrievals of Asian Aerosol Properties During ACE-Asia, *IEEE T. Geosci. Remote*, 44, 3180–3195, 2006.
- Hsu, N. C., Jeong, M.-J., and Bettenhausen, C.: Enhanced Deep Blue aerosol retrieval algorithm: The second generation, *J. Geophys. Res. Atmos.*, 118, 9296–9315, 2013.
- Hu, Y., Vaughan, M., Liu, Z., Lin, B., Yang, P., Flittner, D., Hunt, B., Kuehn, R., Huang, J., Wu, D., Rodier, S., Powell, K., Trepte, C., and Winker, D.: The depolarization-attenuated backscatter relation: CALIPSO lidar measurements vs. theory, *Opt. Express*, 15, 5327–5332, 2007.
- Hu, Y., Winker, D., Vaughan, M., Lin, B., Omar, A., Trepte, C., Flittner, D., Yang, P., Nasiri, S., Baum, B., Sun, W., Liu, Z., Wang, Z., Young, S., Stamnes, K., Huang, J., Kuehn, R., and Holz, R.: CALIPSO/CALIOP cloud phase discrimination algorithm, *J. Atmos. Ocean. Tech.*, 26, 2293–2309, doi:10.1175/2009JTECHA1280.1, 2009.
- Huang, J., Lin, B., Minnis, P., Wang, T., Wang, X., Hu, Y., Yi, Y., and Ayers, J.: Satellite-based assessment of possible dust aerosols semi-direct effect on cloud water path over East Asia, *Geophys. Res. Lett.*, 33, L19802, doi:10.1029/2006GL026561, 2006.
- Huang, J., Minnis, P., Chen, B., Huang, Z., Liu, Z., Zhao, Q., Yi, Y., and Ayers, J.: Long-range transport and vertical structure of Asian dust from CALIPSO and surface measurements during PACDEX, *J. Geophys. Res.*, 113, D23212, doi:10.1029/2008JD010620, 2008.
- Huang, J., Wang, T., Wang, W., Li, Z., and Yan, H.: Climate effects of dust aerosols over East Asian arid and semi-arid regions, *J. Geophys. Res.-Atmos.*, 119, 11398–11416, doi:10.1002/2014JD021796, 2014.
- Huang, L., Jiang, J. H., Tackett, J. L., Su, H., and Fu, R.: Seasonal and diurnal variations of aerosol extinction profile and type distribution from CALIPSO 5-year observations, *J. Geophys. Res.-Atmos.*, 118, 4572–4596, doi:10.1002/jgrd.50407, 2013.
- Huffman, G. J., Adler, R. F., Morrissey, M. M., Bolvin, D. T., Curtis, S., Joyce, R., McGavock, B., and Susskind, J.: Global Precipitation at One-Degree Daily Resolution from Multisatellite Observations, *J. Hydrometeorol.*, 2, 36–50, doi:10.1175/1525-7541(2001)002<0036:GPAODD>2.0.CO;2, 2001.
- Iacono, M. J., Mlawer, E. J., Clough, S. A., and Morcrette, J. J.: Impact of an improved longwave radiation model, RRTM, on the energy budget and thermodynamic properties of the NCAR community climate model, CCM3, *J. Geophys. Res.*, 105, 14873–14890, 2000.
- Jaeglé, L., Quinn, P. K., Bates, T. S., Alexander, B., and Lin, J.-T.: Global distribution of sea salt aerosols: new constraints from in situ and remote sensing observations, *Atmos. Chem. Phys.*, 11, 3137–3157, doi:10.5194/acp-11-3137-2011, 2011.
- Jaffe, D., Anderson, T., Covert, D., Kotchenruther, R., Trost, B., Danielson, J., Simpson, W., Berntsen, T., Karlsdottir, S., Blake, D., Harris, J., Carmichael, G., and Uno, I.: Transport of Asian Air Pollution to North America, *Geophys. Res. Lett.*, 26, 711–714, 1999.
- Janssens-Maenhout, G., Crippa, M., Guizzardi, D., Dentener, F., Muntean, M., Pouliot, G., Keating, T., Zhang, Q., Kurokawa, J., Wankmüller, R., Denier van der Gon, H., Kuenen, J. J. P., Klimont, Z., Frost, G., Darras, S., Koffi, B., and Li, M.: HTAP_v2.2: a mosaic of regional and global emission grid maps for 2008 and 2010 to study hemispheric transport of air pollution, *Atmos. Chem. Phys.*, 15, 11411–11432, doi:10.5194/acp-15-11411-2015, 2015.
- Jethva, H., Torres, O., and Ahn, C.: Global assessment of OMI aerosol single-scattering albedo using ground-based AERONET inversion, *J. Geophys. Res.-Atmos.*, 119, 9020–9040, doi:10.1002/2014JD021672, 2014.
- Kahn, R. A., Nelson, D. L., Garay, M. J., Levy, R. C., Bull, M. A., Diner, D. J., Martonchik, J. V., Paradise, S. R., Hansen, E. G., and Remer, L. A.: MISR Aerosol Product Attributes and Statistical Comparisons With MODIS, *IEEE T. Geosci. Remote*, 47, 4095–4114, 2009.
- Kaufman, Y. J., Tanré, D., Remer, L. A., Vermote, E. F., Chu, A., and Holben, B. N.: Operational remote sensing of tropospheric aerosol over land from EOS moderate resolution imaging spectroradiometer, *J. Geophys. Res.*, 102, 17051–17067, 1997.
- Kaufman, Y. J., Boucher, O., Tanre, D., Chin, M., Remer, L. A., and Takemura, T.: Aerosol anthropogenic component estimated from satellite data, *Geophys. Res. Lett.*, 32, L17804, doi:10.1029/2005GL023125, 2005a.
- Kaufman, Y. J., Koren, I., Remer, L. A., Rosenfeld, D., and Rudich, Y.: The effect of smoke, dust, and pollution aerosol on shallow cloud development over the Atlantic Ocean, *P. Natl. Acad. Sci. USA*, 102, 11207–11212, doi:10.1073/pnas.0505191102, 2005b.
- King, M. D., Kaufman, Y. J., Tanre, D., and Nakajima, T.: Remote Sensing of Tropospheric Aerosols from Space: Past, Present, and Future, *Bull. Am. Meteorol. Soc.*, 80, 2229–2259, 1999.
- Kok, J. F.: A scaling theory for the size distribution of emitted dust aerosols suggests climate models underestimate the size of the global dust cycle, *P. Natl. Acad. Sci. USA*, 108, 1016–1021, doi:10.1073/pnas.1014798108, 2011.
- Koren, I., Kaufman, Y. J., Rosenfeld, D., Remer, L. A., and Rudich, Y.: Aerosol invigoration and restructuring of Atlantic convective clouds, *Geophys. Res. Lett.*, 2, L14828, doi:10.1029/2005GL023187, 2005.
- Lau, K., Ramanathan, V., Wu, G., Li, Z., Tsay, S., Hsu, C., Sikka, R., Holben, B., Lu, D., Tartari, G., Chin, M., Koudelova, P., Chen, H., Ma, Y., Huang, J., Taniguchi, K., and Zhang, R.: The joint

- aerosol-monsoon experiment: A new challenge for monsoon climate research, *Bull. Am. Meteorol. Soc.*, 89, 369–383, 2008.
- Levy, R. C., Remer, L. A., Kleidman, R. G., Mattoo, S., Ichoku, C., Kahn, R., and Eck, T. F.: Global evaluation of the Collection 5 MODIS dark-target aerosol products over land, *Atmos. Chem. Phys.*, 10, 10399–10420, doi:10.5194/acp-10-10399-2010, 2010.
- Levy, R. C., Mattoo, S., Munchak, L. A., Remer, L. A., Sayer, A. M., Patadia, F., and Hsu, N. C.: The Collection 6 MODIS aerosol products over land and ocean, *Atmos. Meas. Tech.*, 6, 2989–3034, doi:10.5194/amt-6-2989-2013, 2013.
- Li, M., Zhang, Q., Kurokawa, J., Woo, J.-H., He, K. B., Lu, Z., Ohara, T., Song, Y., Streets, D. G., Carmichael, G. R., Cheng, Y. F., Hong, C. P., Huo, H., Jiang, X. J., Kang, S. C., Liu, F., Su, H., and Zheng, B.: MIX: a mosaic Asian anthropogenic emission inventory for the MICS-Asia and the HTAP projects, *Atmos. Chem. Phys. Discuss.*, 15, 34813–34869, doi:10.5194/acpd-15-34813-2015, 2015.
- Liang, Q., Jaegle, L., Jaffe, D. A., Weiss-Penzias, P., Heckman, A., and Snow, J. A.: Long-range transport of Asian pollution to the northeast Pacific: Seasonal variations and transport pathways of carbon monoxide, *J. Geophys. Res.*, 109, D23S07, doi:10.1029/2003JD004402, 2004.
- Liu, Z., Vaughan, M. A., Winker, D. M., Hostetler, C. A., Poole, L. R., Hlavka, D., Hart, W., and McGill, M.: Use of probability distribution functions for discriminating between cloud and aerosol in lidar backscatter data, *J. Geophys. Res.*, 109, D15202, doi:10.1029/2004JD004732, 2004.
- Liu, Z., Liu, D., Huang, J., Vaughan, M., Uno, I., Sugimoto, N., Kitaka, C., Trepte, C., Wang, Z., Hostetler, C., and Winker, D.: Airborne dust distributions over the Tibetan Plateau and surrounding areas derived from the first year of CALIPSO lidar observations, *Atmos. Chem. Phys.*, 8, 5045–5060, doi:10.5194/acp-8-5045-2008, 2008.
- Lu, Z., Zhang, Q., and Streets, D. G.: Sulfur dioxide and primary carbonaceous aerosol emissions in China and India, 1996–2010, *Atmos. Chem. Phys.*, 11, 9839–9864, doi:10.5194/acp-11-9839-2011, 2011.
- Malm, W. C., Sisler, J. F., Huffman, D., Eldred, R. A., and Cahill, T. A.: Spatial and seasonal trends in particle concentration and optical extinction in the United States, *J. Geophys. Res.*, 99, 1347–1370, 1994.
- Mao, Y. H., Li, Q. B., Zhang, L., Chen, Y., Randerson, J. T., Chen, D., and Liou, K. N.: Biomass burning contribution to black carbon in the Western United States Mountain Ranges, *Atmos. Chem. Phys.*, 11, 11253–11266, doi:10.5194/acp-11-11253-2011, 2011.
- Mao, Y. H., Li, Q. B., Chen, D., Zhang, L., Hao, W.-M., and Liou, K.-N.: Top-down estimates of biomass burning emissions of black carbon in the Western United States, *Atmos. Chem. Phys.*, 14, 7195–7211, doi:10.5194/acp-14-7195-2014, 2014.
- Martonchik, J. V., David, J. D., Crean, K. A., and Bull, M. A.: Regional Aerosol Retrieval Results From MISR, *IEEE T. Geosci. Remote*, 40, 1520–1531, 2002.
- McKeen, S. A., Wotawa, G., Parrish, D. D., Holloway, J. S., Buhr, M. P., Hubler, G., Fehsenfeld, F. C., and Meagher, J. F.: Ozone production from Canadian wildfires during June and July of 1995, *J. Geophys. Res.*, 107, 4192, doi:10.1029/2001JD000697, 2002.
- Mlawer, E. J., Taubman, S. J., Brown, P. D., Iacono, M. J., and Clough, S. A.: Radiative transfer for inhomogeneous atmospheres: RRTM, a validated correlated-k model for the longwave, *J. Geophys. Res.*, 102, 16663–16682, 1997.
- Painter, T. H., Deems, J. S., Belnap, J., Hamlet, A. F., Landry, C. C., and Udall, B.: Response of Colorado River runoff to dust radiative forcing in snow, *P. Natl. Acad. Sci. USA*, 107, 17125–17130, doi:10.1073/pnas.0913139107, 2010.
- Penner, J. E., Zhang, S. Y., Chin, M., Chuang, C. C., Fechter, J., Feng, Y., Geogdzhayev, I. V., Ginoux, P., Herzog, M., Higurashi, A., Koch, D., Land, C., Lohmann, U., Mischecko, M., Nakajima, T., Pitari, G., Soden, B., Tegen, I., and Stowe, L.: A Comparison of Model- and Satellite-Derived Aerosol Optical Depth and Reflectivity, *J. Atmos. Sci.*, 59, 441–460, 2002.
- Qian, Y., Gustafson, W. I., Leung, L. R., and Ghan, S. J.: Effects of soot-induced snow albedo change on snowpack and hydrological cycle in western United States based on Weather Research and Forecasting chemistry and regional climate simulations, *J. Geophys. Res.*, 114, D03108, doi:10.1029/2008JD011039, 2009.
- Qian, Y., Gustafson Jr., W. I., and Fast, J. D.: An investigation of the sub-grid variability of trace gases and aerosols for global climate modeling, *Atmos. Chem. Phys.*, 10, 6917–6946, doi:10.5194/acp-10-6917-2010, 2010.
- Qian, Y., Yan, H., Hou, Z., Johannesson, C., Klein, S., Lucas, D., Neale, R., Rasch, P., Swiler, L., Tannahill, J., Wang, H., Wang, M., and Zhao, C.: Parametric sensitivity analysis of precipitation at global and local scales in the Community Atmosphere Model CAM5, *J. Adv. Model. Earth Syst.*, 7, 382–411, doi:10.1002/2014MS000354, 2015.
- Randerson, J. T., Chen, Y., van der Werf, G. R., Rogers, B. M., and Morton, D. C.: Global burned area and biomass burning emissions from small fires, *J. Geophys. Res.*, 117, G04012, doi:10.1029/2012JG002128, 2012.
- Remer, L. A. and Kaufman, Y. J.: Aerosol direct radiative effect at the top of the atmosphere over cloud free ocean derived from four years of MODIS data, *Atmos. Chem. Phys.*, 6, 237–253, doi:10.5194/acp-6-237-2006, 2006.
- Remer, L. A., Kaufman, Y. J., Tanre, D., Mattoo, S., Chu, D. A., Martins, J. V., Li, R. R., Ichoku, C., Levy, R. C., Kleidman, R. G., Eck, T. F., Vermote, E., and Holben, B. N.: The MODIS aerosol algorithm, products and validation, *J. Atmos. Sci.*, 62, 947–973, 2005.
- Rienecker, M. M., Suarez, M. J., Gelaro, R., Todling, R., Bacmeister, J., Liu, E., Bosilovich, M. G., Schubert, S. D., Takacs, L., Kim, G.-K., Bloom, S., Chen, J., Collins, D., Conaty, A., da Silva, A., Gu, W., Joiner, J., Koster, R. D., Lucchesi, R., Molod, A., Owens, T., Pawson, S., Pegion, P., Redder, C. R., Reichle, R., Robertson, F. R., Ruddick, A. G., Sienkiewicz, M., and Woollen, J.: MERRA: NASA's Modern-Era Retrospective Analysis for Research and Applications, *J. Climate*, 24, 3624–3648, doi:10.1175/JCLI-D-11-00015.1, 2011.
- Sassen, K.: Indirect climate forcing over the western US from Asian Dust storms, *Geophys. Res. Lett.*, 29, 1465, doi:10.1029/2001GL014051, 2002.
- Schulz, M., Textor, C., Kinne, S., Balkanski, Y., Bauer, S., Bernsten, T., Berglen, T., Boucher, O., Dentener, F., Guibert, S., Isaksen, I. S. A., Iversen, T., Koch, D., Kirkevåg, A., Liu, X., Montanaro, V., Myhre, G., Penner, J. E., Pitari, G., Reddy, S., Seland, Ø., Stier, P., and Takemura, T.: Radiative forcing by aerosols as

- derived from the AeroCom present-day and pre-industrial simulations, *Atmos. Chem. Phys.*, 6, 5225–5246, doi:10.5194/acp-6-5225-2006, 2006.
- Schultz, M., Rast, S., van het Bolscher, M., Pulles, T., Brand, R., Pereira, J., Mota, B., Spessa, A., Dalsren, S., van Noije, T., and Szopa, S.: Emission data sets and methodologies for estimating emissions, RETRO project report D1-6, Hamburg, available at: http://retro-archive.iwk.fz-juelich.de/data/documents/reports/D1-6_final.pdf (last access: 3 May 2016), 2007.
- Schuster, G. L., Dubovik, O., and Holben, B. N.: Angström exponent and bimodal aerosol size distributions, *J. Geophys. Res.*, 111, D07207, doi:10.1029/2005JD006328, 2006.
- Shrivastava, M., Fast, J., Easter, R., Gustafson Jr., W. I., Zaveri, R. A., Jimenez, J. L., Saide, P., and Hodzic, A.: Modeling organic aerosols in a megacity: comparison of simple and complex representations of the volatility basis set approach, *Atmos. Chem. Phys.*, 11, 6639–6662, doi:10.5194/acp-11-6639-2011, 2011.
- Skamarock, W. C., Klemp, J. B., Dudhia, J., Gill, D. O., Barker, D. M., Duda, M. G., Huang, X., Wang, W., and Powers, J. G.: A description of the advanced research WRF version 3, NCAR Tech. Note, NCAR/TN-475 + STR, 8 pp., Natl. Center Atmos. Res., Boulder, Colorado, USA, available at: http://www2.mmm.ucar.edu/wrf/users/docs/arw_v3.pdf (last access: 3 May 2016), 2008.
- Smirnov, A., Holben, B. N., Eck, T. F., Dubovik, O., and Slutsker, I.: Effect of wind speed on columnar aerosol optical properties at Midway Island, *J. Geophys. Res.*, 108, 4802, doi:10.1029/2003JD003879, 2003.
- Stauffer, D. R. and Seaman, N. L.: Use of Four-Dimensional Data Assimilation in a Limited_Area Mesoscale Model. Part I: Experiments with Synoptic-Scale Data, *Mon. Weather Rev.*, 118, 1250–1277, 1990.
- Takemura T., Nakajima, T., Dubovik, O., Holben, B. N., and Kinne, S.: Single-scattering albedo and radiative forcing of various aerosol species with a global three-dimensional model, *J. Climate*, 15, 333–352, 2002.
- Tao, Z., Yu, H., and Chin, M.: Impact of transpacific aerosol on air quality over the United States: A perspective from aerosol-cloud-radiation interactions, *Atmos. Environ.*, 125, 48–60, 2016.
- Textor, C., Schulz, M., Guibert, S., Kinne, S., Balkanski, Y., Bauer, S., Bernsten, T., Berglen, T., Boucher, O., Chin, M., Dentener, F., Diehl, T., Easter, R., Feichter, H., Fillmore, D., Ghan, S., Ginoux, P., Gong, S., Grini, A., Hendricks, J., Horowitz, L., Huang, P., Isaksen, I., Iversen, I., Kloster, S., Koch, D., Kirkevåg, A., Kristjansson, J. E., Krol, M., Lauer, A., Lamarque, J. F., Liu, X., Montanaro, V., Myhre, G., Penner, J., Pitari, G., Reddy, S., Seland, Ø., Stier, P., Takemura, T., and Tie, X.: Analysis and quantification of the diversities of aerosol life cycles within AeroCom, *Atmos. Chem. Phys.*, 6, 1777–1813, doi:10.5194/acp-6-1777-2006, 2006.
- Torres, O., Ahn, C., and Chen, Z.: Improvements to the OMI near-UV aerosol algorithm using A-train CALIOP and AIRS observations, *Atmos. Meas. Tech.*, 6, 3257–3270, doi:10.5194/amt-6-3257-2013, 2013.
- Uno, I., Eguchi, K., Yumimoto, K., Takemura, T., Shimizu, A., Uematsu, M., Liu, Z., Wang, Z., Hara, Y., and Sugimoto, N.: Asian dust transported one full circuit around the globe, *Nat. Geosci.*, 2, 557–560, doi:10.1038/ngeo583, 2009.
- Uno, I., Eguchi, K., Yumimoto, K., Liu, Z., Hara, Y., Sugimoto, N., Shimizu, A., and Takemura, T.: Large Asian dust layers continuously reached North America in April 2010, *Atmos. Chem. Phys.*, 11, 7333–7341, doi:10.5194/acp-11-7333-2011, 2011.
- VanCuren, R. A.: Asian aerosols in North America: Extracting the chemical composition and mass concentration of the Asian continental aerosol plume from long-term aerosol records in the western United States, *J. Geophys. Res.*, 108, 4623, doi:10.1029/2003JD003459, 2003.
- van der Werf, G. R., Randerson, J. T., Giglio, L., Collatz, G. J., Mu, M., Kasibhatla, P. S., Morton, D. C., DeFries, R. S., Jin, Y., and van Leeuwen, T. T.: Global fire emissions and the contribution of deforestation, savanna, forest, agricultural, and peat fires (1997–2009), *Atmos. Chem. Phys.*, 10, 11707–11735, doi:10.5194/acp-10-11707-2010, 2010.
- Veihelmann, B., Levelt, P. F., Stammes, P., and Veeffkind, J. P.: Simulation study of the aerosol information content in OMI spectral reflectance measurements, *Atmos. Chem. Phys.*, 7, 3115–3127, doi:10.5194/acp-7-3115-2007, 2007.
- Wiedinmyer, C., Akagi, S. K., Yokelson, R. J., Emmons, L. K., Al-Saadi, J. A., Orlando, J. J., and Soja, A. J.: The Fire INventory from NCAR (FINN): a high resolution global model to estimate the emissions from openburning, *Geosci. Model Dev.*, 4, 625–641, doi:10.5194/gmd-4-625-2011, 2011.
- Winker, D. M., Hunt, W. H., and McGill, M. J.: Initial performance assessment of CALIOP, *J. Geophys. Res.*, 34, L19803, doi:10.1029/2007GL030135, 2007.
- Winker, D. M., Vaughan, M. A., Omar, A., Hu, Y., Powell, K. A., Liu, Z., Hunt, W. H., and Young, S. A.: Overview of the CALIPSO Mission and CALIOP Data Processing Algorithms, *J. Atmos. Ocean. Tech.*, 26, 2310–2323, doi:10.1175/2009JTECHA1281.1, 2009.
- Yu, H., Chin, M., Remer, L. A., Kleidman, R. G., Bellouin, N., Bian, H., and Diehl, T.: Variability of marine aerosol fine-mode fraction and estimates of anthropogenic aerosol component over cloud-free oceans from MODIS, *J. Geophys. Res.*, 114, D10206, doi:10.1029/2008JD010648, 2009.
- Yu, H., Remer, L. A., Chin, M., Bian, H., Tan, Q., Yuan, T., and Zhang, Y.: Aerosols from Overseas Rival Domestic Emissions over North America, *Science*, 337, 566–569, 2012.
- Yu, H., Chin, M., Bian, H., Yuan, T. L., Prospero, J. M., Omar, A. H., Remer, L. A., Winker, D. M., Yang, Y., Zhang, Y., and Zhang, Z.: Quantification of trans-Atlantic dust transport from seven-year (2007–2013) record of CALIPSO lidar measurements, *Remote Sens. Environ.*, 159, 232–249, doi:10.1016/j.rse.2014.12.010, 2015.
- Yu, H. B., Dickinson, R. E., Chin, M., Kaufman, Y. J., Holben, B. N., Geogdzhayev, I. V., and Mishchenko, M. I.: Annual cycle of global distributions of aerosol optical depth from integration of MODIS retrievals and GOCART model simulations, *J. Geophys. Res.*, 108, 4128, doi:10.1029/2002JD002717, 2003.
- Yu, H. B., Dickinson, R. E., Chin, M., Kaufman, Y. J., Zhou, M., Zhou, L., Tian, Y., Dubovik, O., and Holben, B. N.: Direct radiative effect of aerosols as determined from a combination of MODIS retrievals and GOCART simulations, *J. Geophys. Res.*, 109, D03206, doi:10.1029/2003JD003914, 2004.
- Yu, H. B., Fu, R., Dickinson, R. E., Zhang, Y., Chen, M., and Wang, H.: Interannual variability of smoke and warm cloud relationships in the Amazon as inferred from MODIS retrievals, *Remote*

- Sens. Environ., 111, 435–449, doi:10.1016/j.rse.2007.04.003, 2007.
- Yu, H. B., Remer, L. A., Chin, M., Bian, H. S., Kleidman, R. G., and Diehl, T.: A satellite-based assessment of transpacific transport of pollution aerosol, *J. Geophys. Res.*, 113, D14S12, doi:10.1029/2007JD009349, 2008.
- Yu, H. B., Chin, M., Winker, D. M., Omar, A. H., Liu, Z. Y., Kitaka, C., and Diehl, T.: Global view of aerosol vertical distributions from CALIPSO lidar measurements and GOCART simulations: Regional and seasonal variations, *J. Geophys. Res.*, 115, D00H30, doi:10.1029/2009JD013364, 2010.
- Zaveri, R. A. and Peters, L. K.: A new lumped structure photochemical mechanism for large-scale applications, *J. Geophys. Res.*, 104, 30387–30415, 1999.
- Zaveri, R. A., Easter, R. C., Fast, J. D., and Peters, L. K.: Model for Simulating Aerosol Interactions and Chemistry (MOSAIC), *J. Geophys. Res.*, 113, D13204, doi:10.1029/2007JD008782, 2008.
- Zhang, J. and Reid, J. S.: MODIS aerosol product analysis for data assimilation: Assessment of over-ocean level 2 aerosol optical thickness retrievals, *J. Geophys. Res.*, 111, D22207, doi:10.1029/2005JD006898, 2006.
- Zhang, Q., Streets, D. G., Carmichael, G. R., He, K. B., Huo, H., Kannari, A., Klimont, Z., Park, I. S., Reddy, S., Fu, J. S., Chen, D., Duan, L., Lei, Y., Wang, L. T., and Yao, Z. L.: Asian emissions in 2006 for the NASA INTEX-B mission, *Atmos. Chem. Phys.*, 9, 5131–5153, doi:10.5194/acp-9-5131-2009, 2009.
- Zhao, C., Liu, X., Leung, L. R., Johnson, B., McFarlane, S. A., Gustafson Jr., W. I., Fast, J. D., and Easter, R.: The spatial distribution of mineral dust and its shortwave radiative forcing over North Africa: modeling sensitivities to dust emissions and aerosol size treatments, *Atmos. Chem. Phys.*, 10, 8821–8838, doi:10.5194/acp-10-8821-2010, 2010a.
- Zhao, C., Wang, Y., Yang, Q., Fu, R., and Choi, Y.: Impact of East Asia summer monsoon on the air quality over China: view from space, *J. Geophys. Res.*, 115, D09301, doi:10.1029/2009JD012745, 2010b.
- Zhao, C., Liu, X., Ruby Leung, L., and Hagos, S.: Radiative impact of mineral dust on monsoon precipitation variability over West Africa, *Atmos. Chem. Phys.*, 11, 1879–1893, doi:10.5194/acp-11-1879-2011, 2011.
- Zhao, C., Liu, X., and Leung, L. R.: Impact of the Desert dust on the summer monsoon system over Southwestern North America, *Atmos. Chem. Phys.*, 12, 3717–3731, doi:10.5194/acp-12-3717-2012, 2012.
- Zhao, C., Leung, L. R., Easter, R., Hand, J., and Avise, J.: Characterization of speciated aerosol direct radiative forcing over California, *J. Geophys. Res.*, 118, 2372–2388, doi:10.1029/2012JD018364, 2013a.
- Zhao, C., Chen, S., Leung, L. R., Qian, Y., Kok, J. F., Zaveri, R. A., and Huang, J.: Uncertainty in modeling dust mass balance and radiative forcing from size parameterization, *Atmos. Chem. Phys.*, 13, 10733–10753, doi:10.5194/acp-13-10733-2013, 2013b.
- Zhao, C., Hu, Z., Qian, Y., Ruby Leung, L., Huang, J., Huang, M., Jin, J., Flanner, M. G., Zhang, R., Wang, H., Yan, H., Lu, Z., and Streets, D. G.: Simulating black carbon and dust and their radiative forcing in seasonal snow: a case study over North China with field campaign measurements, *Atmos. Chem. Phys.*, 14, 11475–11491, doi:10.5194/acp-14-11475-2014, 2014.
- Zhao, C., Huang, M., Fast, J. D., Berg, L. K., Qian, Y., Guenther, A., Gu, D., Shrivastava, M., Liu, Y., Walters, S., Pfister, G., Jin, J., Shilling, J. E., and Warneke, C.: Sensitivity of biogenic volatile organic compounds (BVOCs) to land surface parameterizations and vegetation distributions in California, *Geosci. Model Dev. Discuss.*, doi:10.5194/gmd-2015-266, in review, 2016.